

Geochemistry, Geophysics, Geosystems



RESEARCH ARTICLE

10.1029/2023GC011412

Key Points:

- The Leka Ophiolite Complex (LOC) preserves a record of geochemical variation from forearc basaltic to boninitic magmatism, reflecting formation during initiation and early evolution of a subduction zone
- A 491.36 ± 0.17 Ma U-Pb zircon date for an LOC forearc basalt is considered to date subduction initiation in the "Leka sector" of the Iapetus Ocean
- Differences between the LOC pseudostratigraphy and the model Izu-Bonin-Mariana forearc may result from selective preservation of the spatially variable forearc lithosphere in addition to the specific history of formation, obduction, deformation, and uplift/ erosion records

Supporting Information:

Supporting Information may be found in the online version of this article.

Correspondence to:

N. A. Becker, nbecker@jhu.edu; naomiannbecker@gmail.com

Citation

Becker, N. A., Nelson, W. R., Browning-Hanson, J. F., George, F. R., Crowley, J. L., & Viete, D. R. (2024). Forearc variability and the geochemical diversity of suprasubduction zone ophiolites: Insights from the Leka ophiolite complex, Norway. *Geochemistry, Geophysics, Geosystems*, 25, e2023GC011412. https://doi.org/10.1029/2023GC011412

Received 22 DEC 2023 Accepted 12 JUN 2024

Author Contributions:

Conceptualization: Naomi A. Becker, Daniel R. Viete Data curation: Naomi A. Becker

Data curation: Naoini A. Decker

© 2024 The Author(s). Geochemistry, Geophysics, Geosystems published by Wiley Periodicals LLC on behalf of American Geophysical Union.

This is an open access article under the terms of the Creative Commons Attribution-NonCommercial-NoDerivs License, which permits use and distribution in any medium, provided the original work is properly cited, the use is non-commercial and no modifications or adaptations are made.

Forearc Variability and the Geochemical Diversity of Suprasubduction Zone Ophiolites: Insights From the Leka Ophiolite Complex, Norway

Naomi A. Becker¹, Wendy R. Nelson², Joseph F. Browning-Hanson¹, Freya R. George^{1,3}, James L. Crowley⁴, and Daniel R. Viete¹

¹Department of Earth & Planetary Sciences, Johns Hopkins University, Baltimore, MD, USA, ²Department of Physics, Astronomy and Geosciences, Towson University, Towson, MD, USA, ³School of Earth Sciences, University of Bristol, Bristol, UK, ⁴Department of Geosciences, Boise State University, Boise, ID, USA

Abstract New whole-rock major and trace element geochemistry from the Leka Ophiolite Complex in Norway is presented and compared to the geochemical evolution and proposed tectonomagmatic processes recorded in the Izu-Bonin-Mariana system. These data demonstrate that the Leka Ophiolite Complex formed as forearc lithosphere during subduction initiation. A new high-precision zircon U-Pb date on forearc basalt constrains the timing of subduction initiation in the "Leka sector" of the Iapetus Ocean to 491.36 ± 0.17 Ma. The tectonomagmatic record of the Leka Ophiolite Complex captures only the earliest stages of subduction initiation and is thereby distinct from some other Appalachian–Caledonian ophiolites of similar age. The diversity of Appalachian–Caledonian ophiolite records may represent differing preservation and exposure of a variable forearc lithosphere.

Plain Language Summary The Leka Ophiolite Complex (LOC) represents a preserved fragment of oceanic crust that formed during subduction in the Iapetus Ocean. Geochemical information recorded in the LOC rocks shows that it formed during the initial phase of subduction. The age of subduction initiation in the Iapetus Ocean is estimated at 491.36 million years ago based on isotopic dating of minerals within the LOC rocks. Other fragments of preserved oceanic crust with similar ages are found in the Appalachian—Caledonian mountains; however, their geochemical information suggests that they may have formed during different stages of the subduction zone development. We consider the variations in the oceanic crustal record to reflect selective preservation of different parts of the variable oceanic crust formed during the development of a subduction zone in the Iapetus Ocean.

1. Introduction

Plate tectonics are intrinsically linked to the formation and destruction of oceans. The only accessible physical records of past oceans are ophiolite complexes, making them highly valuable features for the study of plate tectonic processes. Orogenic ophiolites mark ocean suture zones and commonly record geochemistry that reflects a history of both seafloor spreading and subduction zone processes, suggesting that they preserve oceanic lithosphere formed in supra-subduction zone (SSZ) settings (Pearce et al., 1984). The specific histories recorded in ophiolites likely result from selective preservation of SSZ settings that are especially well-primed for obduction (Stern & Bloomer, 1992; Stern et al., 2012; Whattam & Stern, 2011). However, orogenic ophiolites are typically also heavily tectonized, resulting in preservation and exposure of a fraction of the obducted material. The SSZ ophiolite variability—even along a single suture—is dependent upon the nature of the ophiolite itself, which segment of the spatially heterogeneous forearc lithosphere is sampled, and how much of that segment is preserved during subsequent tectonism and exhumation. To contextualize SSZ ophiolites within their broader subduction zone setting, an intact example of oceanic lithosphere formed during subduction zone initiation and development —such as the Izu-Bonin-Mariana (IBM) subduction zone in the western Pacific—can provide a framework for assessing the geochemical records preserved in SSZ ophiolites.

The presence of ocean-scale (1000s of km long) belts of orogen-hosted SSZ ophiolites of similar age is a hallmark of Phanerozoic plate tectonics (e.g., Shafaii Moghadam et al., 2013; Zhou et al., 2018). The Paleozoic Appalachian–Caledonian mountains host a >6,500 km SSZ ophiolite belt spanning the southeastern United States to northern Norway and Sweden and may record the rapid initiation of an extensive subduction zone within the

BECKER ET AL. 1 of 20



Funding acquisition: Naomi A. Becker, Daniel R. Viete

Investigation: Naomi A. Becker, Joseph F. Browning-Hanson, James L. Crowley Project administration: Daniel R. Viete Supervision: Daniel R. Viete Validation: Naomi A. Becker, Wendy R. Nelson, Joseph F. Browning-Hanson, Freya R. George, James L. Crowley, Daniel R. Viete

Visualization: Naomi A. Becker Writing – original draft: Naomi A. Becker

Writing – review & editing: Naomi A. Becker, Wendy R. Nelson, Joseph F. Browning-Hanson, Freya R. George, James L. Crowley, Daniel R. Viete Iapetus Ocean (Bird et al., 1971, 1971; Dilek & Furnes, 2011 and references therein). This study uses the detailed record of tectonomagmatic evolution preserved in the IBM forearc as a model to demonstrate that the Leka Ophiolite Complex (LOC)—a SSZ ophiolite in the Norwegian Caledonides—records subduction initiation in the Iapetus Ocean. We hypothesize that the observed geochemical variations in similarly aged Appalachian—Caledonian SSZ ophiolites result from selective preservation and exposure of spatially and temporally diverse portions of the forearc lithosphere.

1.1. Geologic Background

The Scandinavian Caledonides (Figure 1a)—formed during the collision of Laurentia and Baltica—are exposed over >2,000 km of Norway and western Sweden (Andresen, 1988; Gee et al., 2008). The Norwegian Caledonides are composed of a series of thrust sheets emplaced onto the basement and cover sequences of Baltica (Titus et al., 2002). The Lower and Middle Allochthons represent the extended continental margin of Baltica and form the base of the thrust sheets (Andresen, 1988; Gee et al., 2008). The overlying Upper and Uppermost Allochthons contain Iapetan-derived rocks, including ophiolites, volcanic arcs, and—in the Uppermost Allochthon—rocks of Laurentian affinity (Andresen, 1988; Gee et al., 2008). The emplacement of these allochthons is a result of Ordovician accretion at the Laurentian margin, followed by transfer of the peri-Laurentian terranes to Baltica during westward dipping partial subduction of Baltica beneath the Laurentian margin (Andresen, 1988; Gee et al., 2008; Pedersen et al., 1988).

The LOC comprises the island of Leka and the adjacent islets of Madsøya, Frøvikøya, and Storøya (Figure 1b) and is part of the Sauren-Torghatten Nappe of the Helgeland Nappe Complex, which forms the structurally highest portion of the Uppermost Allochthon (McArthur et al., 2014). Full ophiolite pseudostratigraphy has been documented in the LOC (Furnes et al., 1988), including a 1-1.5 km-thick section of the harzburgitic upper mantle and the petrologic Moho (Figure 1b; Albrektsen et al., 1991; Maaløe, 2005). A major northeast-southwest trending low-angle normal fault (Figure 1b) separates the mantle harzburgites from a layered suite of igneous units, which grades southeastward from layered dunite and pyroxenite to layered gabbro, leucogabbro, and anorthosite (Michels et al., 2018; Prestvik, 1980). Massive gabbro is found farther to the southeast on Leka and on the western half of the adjacent island of Madsøya (Prestvik, 1980). A sheeted dike complex of microgabbro and amphibolite is present on eastern Madsøya along with basaltic flows and pillow basalt (Prestvik, 1980). Plagiogranite and keratophyre have been reported on Madsøya and the northeastern portion of Leka (Prestvik, 1980) adjacent to the metasedimentary Skei Group that unconformably overlies the LOC units (Sturt et al., 1985). The igneous LOC units have been metamorphosed to upper greenschist and lower amphibolite facies conditions (Prestvik, 1980), have been folded into a synformal structure plunging to the northeast, and are situated in a postorogenic pull-apart structure. The LOC is assumed to be in tectonic contact with the surrounding country rocks, although contacts are underwater (Furnes et al., 1988; Michels et al., 2018; Titus et al., 2002).

Mafic extrusive and shallow intrusive units on Madsøya have been classified as mid-ocean ridge basalts, island arc tholeites, and boninites, a geochemical variation characteristic of subduction zone forearc magmatism (Furnes et al., 1988). On Storøya, the mafic rocks are more alkaline in character and are suggested to record LOC volcanism distal from the subduction zone, possibly in a backarc basin or at an anomalous ridge segment (Furnes et al., 1988; Prestvik, 1985; Tveit et al., 1993). Re-Os geochronology on LOC harzburgites revealed two episodes of melt extraction (Haller et al., 2021; O'Driscoll et al., 2015, 2021): the first at 589 ± 15 Ma possibly related to the opening of the Iapetus Ocean (and formation of the Storøya basalts), and the second at 485 ± 32 Ma associated with melt extraction during the LOC formation (Haller et al., 2021; O'Driscoll et al., 2015, 2021). The latter date is within error of a 497 ± 2 Ma date for the LOC, as determined by zircon U-Pb dating of keratophyre from the uppermost stratigraphic LOC section (Dunning & Pedersen, 1988). Detrital zircon analyses of the Havna metagraywacke overlying the LOC record two pulses of magmatism: an older peak at c. 550–510 Ma, potentially related to rifting of Rodinia, and a dominant population at c. 500–480 Ma that may be associated with the formation of the LOC (McArthur et al., 2014).

While the origin of the LOC was initially linked to island arc and backarc basin formation (Furnes et al., 1988; Prestvik, 1980), a forearc origin has also been hypothesized (Dunning & Pedersen, 1988) and is more likely based on ophiolite obduction geometries (Stern et al., 2012). The similarity in the LOC magmatic products to those documented from the IBM forearc region indicates that the subduction initiation history recorded by the IBM may be a suitable proxy for the LOC development (Furnes et al., 1988).

BECKER ET AL. 2 of 20

15252027, 2024, 7, Downloaded from https://agapubs.onlinelbrary.wiley.com/doi/10.1029/2023GC011412 by Dainel Videe - Johns Hopkins University, Wiley Online Library on [11/07/2024]. See the Terms and Conditions (https://onlinelbrary.wiley.com/terms

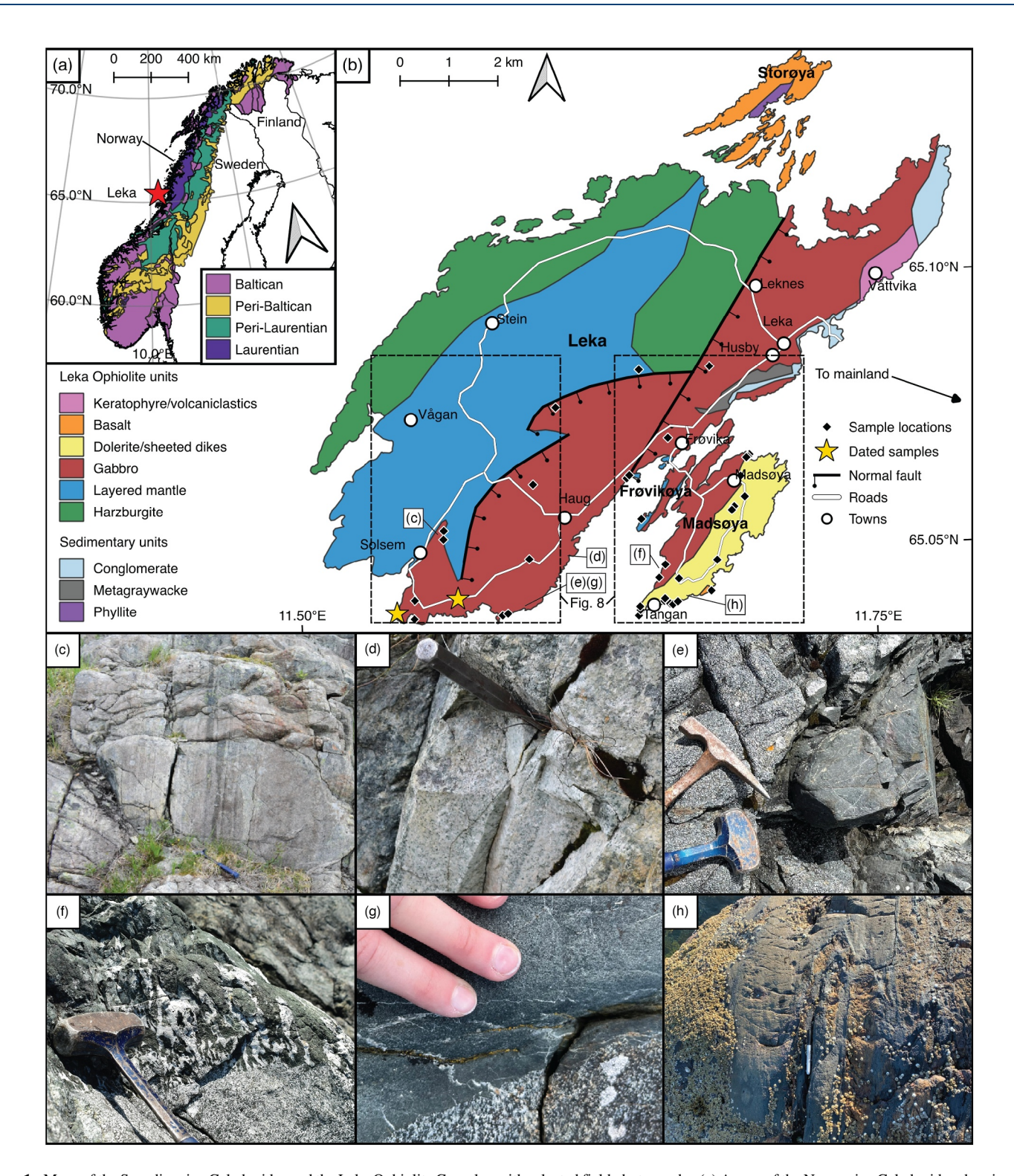


Figure 1. Maps of the Scandinavian Caledonides and the Leka Ophiolite Complex with selected field photographs. (a) A map of the Norwegian Caledonides showing the major terranes/allochthons (adapted from Roberts, 1988). Red star shows the position of the island of Leka. (b) Bedrock and sampling map of the Leka Ophiolite Complex (modified from Michels et al., 2018; Prestvik, 1980). Field images of (c) layered igneous units; (d) anorthosite; (e) a mafic dike within a coarse-grained mafic host; (f) pegmatitic contact between the mafic dike and coarse-grained mafic host; (g) chilled margin on a mafic dike; and (h) pillow basalt on Madsøya. Locations of the field images are shown in (b).

BECKER ET AL. 3 of 20

2. Samples and Field Relationships

Forty samples of mafic rocks were obtained from LOC outcrops on the islands of Leka, Madsøya, and Frøvikøya (Figure 1b). Thirteen are medium- to coarse-grained intrusive rocks collected from the mapped gabbro region on Leka (Prestvik, 1980), which vary within an outcrop from metagabbro to metaleucogabbro and meta-anorthosite (Figure 1c).

The remaining 27 samples are fine- to medium-grained mafic rocks collected from mafic shallow intrusive units and mafic extrusive units on Leka (n = 7), Madsøya (n = 19), and Frøvikøya (n = 1) (Figure 1b). On the southern coast of Leka, the finer-grained mafic rocks were sampled from dikes and igneous bodies that ranged from tens of centimeters to several meters in width and were hosted within coarser-grained mafic rocks (Figure 1e). Contacts between the finer-grained and coarser-grained mafic units sporadically display pegmatitic margins of green amphibole and plagioclase (Figure 1f) and commonly display chilled margins (Figure 1g). The mafic units on the western coast of Madsøya exhibit the same characteristics as those on the southern coast of Leka. On the eastern side of Madsøya, finer-grained mafic units dominate the lithology and display multiple cross-cutting generations of microgabbroic dikes within a single outcrop. To the southeast on Madsøya, the finer-grained mafic units resemble lava flows and pillow basalts are present on the coast near Tangan (Figure 1h).

3. Analytical Methods

3.1. Bulk-Rock Major and Trace Element Geochemistry

Weathering products were removed from samples prior to crushing and powdering. Powders were mixed with lithium tetraborate, flux melted, and then quenched to create glass discs at the Franklin and Marshall X-Ray Laboratory, where analysis of bulk-rock major-element composition was determined by a Malvern PAN-alytical, Inc. Zetium X-ray fluorescence (XRF) spectrometer.

Fragments of the glass discs were mounted in 1" epoxy rounds, polished, and analyzed for trace-element composition at Johns Hopkins University (JHU). A Teledyne-Cetac Analyte G2 193 nm laser equipped with a two-volume HelEx II ablation cell coupled to an Agilent 8900 quadrupole ICP-MS was used for laser ablation inductively coupled plasma mass spectrometry (LA-ICP-MS). Analytical settings for bulk-rock geochemistry by LA-ICP-MS are provided in Table S1 in Supporting Information S1. The LOC glasses were measured in triplicate, with reference materials measured after every seven unknowns. Iolite v4 was used for data reduction (Paton et al., 2011), with the XRF-determined Ca concentration employed as the internal standard.

3.2. Geochronology

Samples were prepared for zircon U-Pb analysis by crushing and sieving to a <500 µm fraction that was subsequently washed to remove clay-sized particles. The resulting fraction was subjected to Frantz magnetic separation then density separation using a sodium polytungstate (SPT) heavy liquid medium (following the method of Andò, 2020). Hand-picked zircons were annealed in a muffle furnace for 60 hr at 900°C, mounted in 1" epoxy rounds, and polished to expose grains. Polished mounts were imaged in cathodoluminescence (CL) using a Deben Centaurus CL detector mounted on a Thermo Scientific Helios G4 UC scanning electron microscope (SEM) in the Materials Characterization and Processing Facility, JHU.

Initial U-Pb geochronology analysis of mounted and imaged zircons was performed using the LA-ICP-MS instrumentation described in Section 3.1 and geochronology analytical settings detailed in Table S1 in Supporting Information S1. Six isotopes (204 Pb, 206 Pb, 207 Pb, 208 Pb, 232 Th, and 238 U) were measured and standard reference materials were measured after every nine unknown analyses. Reference material 91500 (1,063.6 \pm 0.3 Ma: Wiedenbeck et al., 1995; Schoene et al., 2006) was used as the primary standard for data reduction, and analyses on Plešovice (337.13 \pm 0.37 Ma: Sláma et al., 2008) and Temora II (416.78 \pm 0.33 Ma: Black et al., 2004) were used to assess performance. Data reduction was completed in iolite v4 using a median fit to the standard data and including the U-Pb zircon geochronology down-hole fractionation correction of Paton et al. (2010, 2011). An excess uncertainty of 2% was added in quadrature to isotope ratio values obtained from data reduction in iolite v4, as required to obtain in-session "single population" statistics for secondary and tertiary reference materials, which were assumed to be homogeneous in isotopic composition (see method of Horstwood et al., 2016). Weighted mean dates for standards and unknowns were calculated using IsoplotR

BECKER ET AL. 4 of 20

(Vermeesch, 2018) and are provided at 2s. The statistical term s (sample standard deviation) is used in place of σ (population standard deviation), as recommended by Horstwood et al. (2016).

Chemical abrasion isotope dilution thermal ionization mass spectrometry (CA-ID-TIMS) analyses were performed at Boise State University (BSU). Uranium and Pb isotopic measurements were made using a GV Isoprobe-T multicollector TIMS equipped with an ion-counting Daly detector. Sectioned zircon grains were selected based on CL images and LA-ICP-MS data and removed from epoxy mounts for analysis. The zircons were chemically abraded, cleaned, and then spiked with the mixed $^{233}\text{U}-^{205}\text{Pb}$ tracer solution (BSU-1B) prior to U and Pb extraction from the zircon matrix using HCl-based anion-exchange chromatography (Krogh, 1973). The U and Pb were eluted and dried with 2 μ l of 0.05 N H₃PO₄ and loaded on a single outgassed Re filament in 5 μ l of a silica-gel/phosphoric acid mixture (Gerstenberger & Haase, 1997). U-Pb dates and uncertainties were calculated using the algorithms of Schmitz and Schoene (2007) along with calibration of the BSU-1B tracer ($^{235}\text{U}/^{205}\text{Pb}$ of 77.93 and $^{233}\text{U}/^{235}\text{U}$ of 1.007066), U decay constants of Jaffey et al. (1971) and a $^{238}\text{U}/^{235}\text{U}$ of 137.818 (Hiess et al., 2012). $^{206}\text{Pb}/^{238}\text{U}$ ratios and dates were corrected for initial ^{230}Th disequilibrium using $D_{\text{Th/U}} = 0.20 \pm 0.05$ (1 σ) and the algorithms of Crowley et al. (2007). A weighted mean $^{206}\text{Pb}/^{238}\text{U}$ date was calculated from equivalent dates (probability of fit >0.05) using Isoplot 3.0 (Ludwig, 2003a, 2003b), with error reported at the 95% confidence interval.

3.3. Petrography

The medium- to coarse-grained mafic rocks (metagabbro, metaleucogabbro, and meta-anorthosite; n=13) are altered to a fine-grained felty groundmass of cryptocrystalline quartz and plagioclase mixed with talc and serpentine. Colorless to light green anhedral corroded amphiboles have been variably altered to fine-grained chlorite. Epidote and rutile are the primary accessory minerals, and the samples contain <1 modal% opaques. The metagabbro samples (Figure 2a) have \geq 45 modal% amphibole (and alteration products), the metaleucogabbros have 30–40 modal% amphibole, and the meta-anorthosites (Figure 2b) have \leq 10 modal% amphibole.

The finer-grained mafic rocks are amphibolites and are split into four groups based on petrography (Table 1). Group 1 amphibolites (Figure 2c; n = 13) contain 30–70 modal%, <0.5 mm, semi-equant, prismatic, moderately aligned amphiboles that exhibit yellow-green-blue pleochroism, with up to 30 modal% alteration to chlorite and interstitial microcrystalline plagioclase comprises 20–45 modal% of the samples. Opaques (up to 5 modal%) occur as discrete euhedral grains or as anhedral clusters. Sample LO22-48 has 5 modal% biotite.

Group 2 amphibolites (Figure 2d; n=8) contain 35–60 modal% amphibole and 30–50 modal% plagioclase. Two samples (LO22-44, LO22-06B) have 5–10 modal% biotite. They contain <0.5 mm tabular amphiboles that show minor alteration to chlorite and are aligned to define a mineral lineation. Interstitial plagioclase (30–45 modal%) displays a "dusty" alteration texture from sericitization. Group 2 amphibolites contain 5–10 modal% opaques, which occur as euhedral grains or anhedral clusters.

Group 3 amphibolites (Figure 2e; n=2) consist of 40–45 modal%, \sim 1 mm, yellow-green-blue pleochroic, tabular-to-needle-like amphiboles that are semi-aligned within a mineral lineation. They contain 45–50 modal% interstitial microcrystalline plagioclase and 5 modal% opaques, which present as euhedral clusters of polygonal grains or as anhedral clusters. Sample AL22-47 contains 10 modal% biotite.

Group 4 amphibolites (Figure 2f; n=4) contain 40–50 modal% amphibole and 45–55 modal% plagioclase. Sample LO19-43 has 10 modal% biotite. The samples have ≤ 1 mm, tabular amphibole crystals that exhibit yellow-green-blue pleochroism and define a strong mineral lineation. Interstitial plagioclase has a "dusty" alteration texture, and ≤ 5 modal% accessory opaques occur as euhedral grains or anhedral clusters with size variation between samples.

3.4. Bulk-Rock Major and Trace Element Geochemistry

In Figure 3 the bulk-rock major and trace element geochemistry data for the fine- to medium-grained LOC rocks are plotted alongside published data (Ishizuka et al., 2011; Pearce & Reagan, 2019; Reagan et al., 2010, 2019; Shervais et al., 2021) for IBM forearc basalts (IBM FAB), IBM high-magnesium andesites (IBM HMA), and IBM boninites (IBM BON). The medium- to coarse-grained mafic samples (metagabbros, metaleucogabbros, and meta-anorthosites) were excluded as they were determined to be cumulate in nature and thereby differ from the

BECKER ET AL. 5 of 20

from https://agupubs.onlinelibrary.wiley.com/doi/10.1029/2023GC011412 by Daniel Viete - Johns Hopkins University, Wiley Online Library on [11/07/2024]. See the Terms and Condition

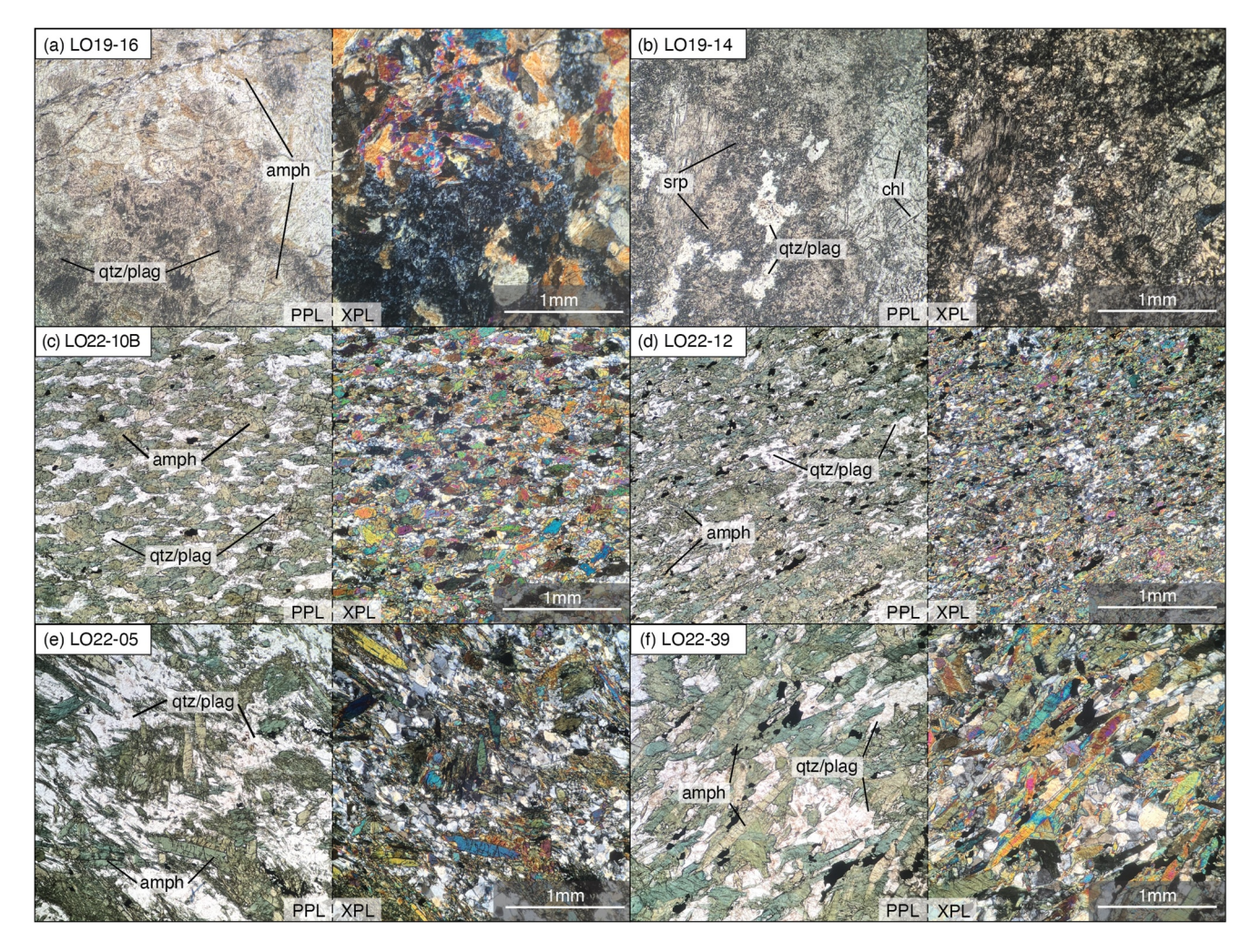


Figure 2. Photomicrographs representing examples of rock types described in the text. (a) Metagabbro; (b) anorthosite; (c) Group 1 amphibolite; (d) Group 2 amphibolite; (e) Group 3 amphibolite; (f) Group 4 amphibolite. Abbreviations: amph = amphibole; chl = chlorite; qtz = quartz; plag = plagioclase; srp = serpentine.

non-cumulate IBM rocks on which the classification scheme was developed. Values of bulk-rock major and trace element concentrations for all fine- to medium-grained (non-cumulate) rocks of this study are provided in Table 2.

The non-cumulate mafic LOC samples overlap with IBM FAB for all major elements except Na₂O, which occurs at significantly higher concentrations in LOC samples than in IBM FAB samples (Figure 3a). Major elements in LOC samples show no correlation with MgO content except for Fe₂O₃, TiO₂, CaO and P₂O₅, which all show minor to moderate negative correlations with MgO ($R^2 = 0.52, 039, 0.24, and 0.37, respectively$). The range of MgO (4–11 wt.%) and trends of Fe₂O₃, Al₂O₃, TiO₂, MnO, CaO, K₂O, and P₂O₅ match those of IBM FAB and IBM HMA, though a few samples from the LOC show minor overlap with IBM BON at MgO >8 wt.%. Four samples have higher K₂O than the rest of the LOC samples but are still within the range for IBM FAB and IBM HMA.

Highly immobile elements (Zr, Nb, and Y) in LOC samples (Figure 3b) display negative correlations with MgO ($R^2 = 0.30, 0.53, 0.34$, and 0.37, respectively). Four samples have MgO >8 wt.% and record Zr and Nb abundances that overlap with IBM BON series samples; however, the Yb and Y concentrations are higher than those for the IBM BON. The LOC samples have positive to negative heavy REE (HREE) slopes ([Gd/Lu]_{N-MORB} = 0.63–1.03), positive to negative light REE (LREE) slopes ([La/Sm]_{N-MORB} = 0.44–1.52), and positive to flat slopes across all REEs ([La/Lu]_{N-MORB} = 0.26–1.02).

The LOC samples plot along the tholeitic trend on the alkalis-iron-magnesium (AFM) volcanic classification diagram of Irvine and Baragar (1971); only two samples plot along a calc-alkaline trend (Figure 3c), consistent

BECKER ET AL. 6 of 20

Table 1

Modal Mineralogy for LOC Samples of '

Sample	Rock type	Group	Amphibole	Plagioclase	Chlorite	Serpentine	Opaques	Biotite	Accessory mineral(s)
LO19-16	Metagabbro		45	45		10			
LO19-37	Metagabbro		45	30	25				Epidote
LO19-20	Metagabbro		50	30		20			
LO19-06	Metaleucogabbro		30	10	30	30			Rutile
LO19-17	Metaleucogabbro		35	30	15	20			
LO19-12	Metaleucogabbro		40	40	10	10			
LO19-31	Metaleucogabbro		40	60					
LO19-09	Metaleucogabbro		40	35	10	15			
LO19-42	Meta-anorthosite		10	50	40				Calcite
LO19-30	Meta-anorthosite		10	90					
LO19-10	Meta-anorthosite			85		15			
LO19-14	Meta-anorthosite			85		15			
LO19-40	Meta-anorthosite			50	40	10			
LO19-22b	Amphibolite	1	30	35	30		5		
LO19-38	Amphibolite	1	30	45	20		5		
LO22-32	Amphibolite	1	45	30	20		5	<1	Calcite
LO19-15	Amphibolite	1	50	20	30				Zoisite
LO22-13	Amphibolite	1	50	45			5		
LO22-18	Amphibolite	1	50	45			5		Calcite
LO22-19A	Amphibolite	1	50	45			5		
LO22-23	Amphibolite	1	50	45		2	3		
LO22-48	Amphibolite	1	50	40			5	5	
LO19-25	Amphibolite	1	55	35	5		5		Rutile
LO22-10B	Amphibolite	1	60	40			<1		
LO22-24	Amphibolite	1	60	35			5		
LO19-36a	Amphibolite	1	70	30			<1		
LO22-44	Amphibolite	2	35	45			10	10	
LO22-34	Amphibolite	2	45	30	20		5	<1	Calcite
LO22-37	Amphibolite	2	45	50	<1		5		
LO22-15A	Amphibolite	2	50	40			10		Rutile
LO22-30	Amphibolite	2	50	40			10		Calcite
LO22-06B	Amphibolite	2	60	30			5	5	
LO22-12	Amphibolite	2	60	30			10		
LO22-41	Amphibolite	2	60	35			5		
LO22-47	Amphibolite	3	40	45			5	10	
LO22-05	Amphibolite	3	45	50			5		
LO22-42	Amphibolite	4	40	55			5		
LO19-43	Amphibolite	4	40	50			<1	10	
LO22-11B	Amphibolite	4	50	45			5		
LO22-39	Amphibolite	4	50	45			5		

with an observed tholeitic trend for IBM FAB and calc-alkaline trend for IBM BON. The immobile element discrimination scheme of Winchester and Floyd (1977), which uses Nb/Y versus Zr/TiO₂, classifies all LOC samples as sub-alkaline basalt or andesite/basalt (Figure 3d).

BECKER ET AL. 7 of 20

1525207, 2024, 7, Downloaded from https://gupubs.onlinelibrary.wiley.com/doi/10.1029/2023/GC011412 by Daniel Vide - Johns Hopkins University, Wiley Online Library on [11/07/2024]. See the Terms and Conditions (https://onlinelibrary.wiley.com/terms-and-conditions) on Wiley Online Library for rules of use; O.A articles as governed by the applicable Creat

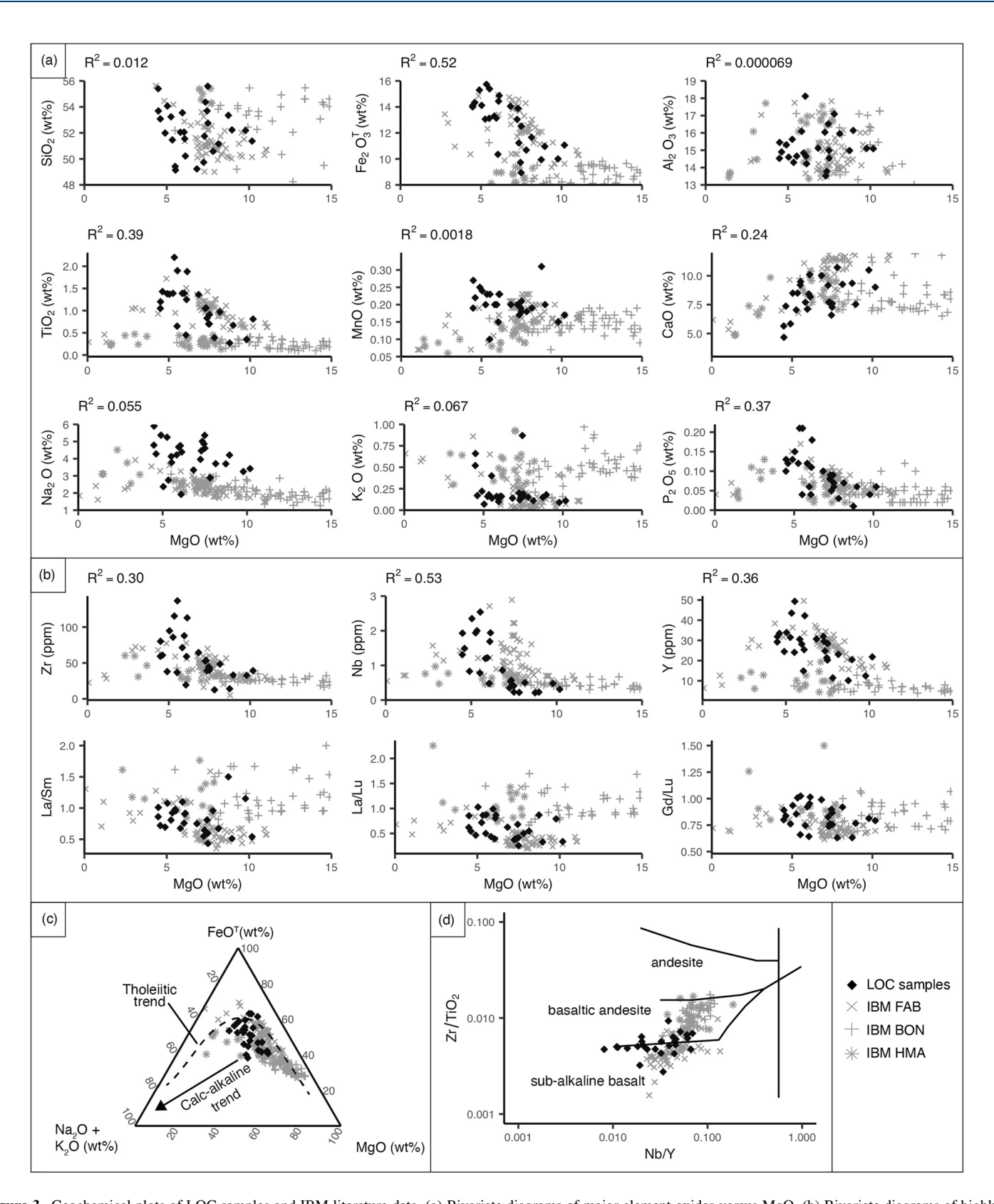


Figure 3. Geochemical plots of LOC samples and IBM literature data. (a) Bivariate diagrams of major element oxides versus MgO. (b) Bivariate diagrams of highly immobile elements (Zr, Nb, Y) and select trace element ratios (La/Sm, La/Lu, Gd/Lu) versus MgO. (c) Alkalis-iron-magnesium (AFM) diagram for volcanic series classification (after Irvine & Baragar, 1971). (d) Immobile element classification diagram (after Winchester & Floyd, 1977). Literature IBM data are from Ishizuka et al. (2011), Pearce and Reagan (2019), Reagan et al. (2010, 2019), and Shervais et al. (2021).

BECKER ET AL. 8 of 20

 Table 2

 Bulk Rock Major and Trace Element Concentrations for Non-Cumulative LOC Samples of This Study Used in Classifications

1	Latitude (°N)	11.54146	11.68159					-1 · · ·		11.69734 1	11.6967 11			11.69457 11.	11.58727 11.5	11.58961 11.6623		11.54894 11.64643		726 11.64714	714 11.65193	93 11 66452	52 11 65786		18 11.66031	11.66367	
1	Longitude ("W) Classification	65.04082 E-FAB			4	st	_	-																		57 65.0408	
1	nalyses (wt%)																										
	SiO2	1 0	1 30	1.36	52.18	53.08	49.42	51.75																			
1 1 1 1 1 1 1 1 1 1	AI203	14.66	15.63	15.12	15.11	6.41	19.28	13.52																			
Column C	e203T	15.39	13.06	14.05	10	14.34	13.12	13,88																			
Column C	MnO	0.23	0.2	0.2	0.15	0.22	0.1	0.59																			
1, 1, 1, 1, 1, 1, 1, 1, 1, 1, 1, 1, 1,	MgO	5.53	5.26	6.83	9.78	4.61	5.51	7.29																			
No.	CaO	9.49	7.04	10.02	10.49	7.37	9.2	7.7																			
No. Control	Va2O	3.78	5.25	3.34	3.25	4.28	4.13	4.46																			
Column C	K20	0.14	0.16	0.14	0.09	0.17	0.4	0.12																			
No.	205	0.21	0.12	0.1	0.04	0.12	0.04	60.0																			
Mart	[O	0.47	1.34	0.4	1.43	0.51	1.81	0.47																			
No.	analyses	(Ma																									
State Stat		AN	NA	NA	NA	NA	NA	ľ			"	L				Ι΄			ľ	L		l		ı	Ľ		76.84
State Stat	Sc	49.89	43.33	50.92	48.78	51.05	53.36																				51.56
	>	480.4	476.25	451.07	292.68	551,64	471.54			.,	•		7				•		.,	_							259.2
Name	<u>ن</u>	55.34	12.09	58.08	412.94	24.53	20.39																				224.6
1. 1. 1. 1. 1. 1. 1. 1.	3 Z	23.47	17.89	24.99	84.65	15.81	13.71																				31.32
1. 1. 1. 1. 1. 1. 1. 1.	: ∂	46.25	465.7	9.16	7.78	53.31	2530.52																				78.61
1.1 1.1	Zu	102.96	82.37	76.28	53.84	94.24	39.72																				63.96
State Contact Contac	Rb	1.68	0.64	1.31	0.71	3.65	7.02	0.95																			1.88
	ან >	78.16	81.82	99.34	88.46	109.58	147.72	86.79																			88.03
0.00 0.00 0.00 0.00 0.00 0.00 0.00 0.0	7.	136.54	31.31	50.71	32.66	53.46	36.91	53.58																			14.01
14.1 1. 1. 1. 1. 1. 1. 1. 1. 1. 1. 1. 1. 1	QN.	2.54	1.94	98.0	0.48	1.49	0.78	0.54																			0.21
1, 1, 1, 1, 1, 1, 1, 1, 1, 1, 1, 1, 1,	Cs	0.05	0,02	60.0	0.01	0.17	0.5	0,05																			0,14
1. 1. 1. 1. 1. 1. 1. 1.	Ba	17.12	17.15	13.05	16.39	19.33	83.72	14.35																			105.3
1. 1. 1. 1. 1. 1. 1. 1.	ا ت	18.37	11 15	8.06	4.32	20.7	5.5	5.44																			3.59
6.29 3.47 8.61 3.64 3.64 4.23 1.56 4.29 1.59 4.29 4.29 1.59 4.29 4.29 1.59 4.29 1.59 4.29 1.59 4.59 4.29 1.59 4.29 1.59 4.59 1.59 4.49 4.59 1.59 4.69 4.59 1.59 4.69 4.59 6.59 6.59 6.59 1.59 4.69 4.59 6.59 <th< td=""><td>3 &</td><td>3.23</td><td>1.82</td><td>1.44</td><td>0.69</td><td>1.58</td><td>0.74</td><td>1.06</td><td></td><td></td><td></td><td></td><td></td><td></td><td></td><td></td><td></td><td></td><td></td><td></td><td></td><td></td><td></td><td></td><td></td><td></td><td>0.43</td></th<>	3 &	3.23	1.82	1.44	0.69	1.58	0.74	1.06																			0.43
1.14 3.22 1.14 3.22 1.15 3.24 3.24 3.24 3.15 3.24 3.15 3.24 3.24 3.15 3.24 3.24 3.15 3.24 3.24 3.24 3.24 3.24 3.24 3.24 3.24	PN	16.56	9.57	8.28	3,37	8,61	3,61	6,11																			1.97
1.1. 1.1. 1.1. 1.1. 1.1. 1.1. 1.1. 1.1	Sm	5.33	3.61	2.79	1.14	3.22	1.68	2.27																			0.76
4.3 1.7 4.8 5.2 1.7 4.8 1.7 2.8 3.2 1.7 4.8 1.7 2.8 3.2 1.7 2.8 3.2 1.7 2.8 3.2 1.7 2.8 3.2 1.7 3.8 3.8 3.8 4.8 3.2 1.7 3.8 4.8 4.8 3.2 1.7 3.8 4.8 4.8 3.2 1.8 4.8 4.8 4.8 4.8 4.8 4.8 4.8 4.8 4.8 4.8 4.8 4.8 4.8 4.8 4.8 4.8 5.8 4.4 2.3 3.2 1.8 6.8 3.4 2.2 1.6 6.8 1.1 6.8 1.1 6.8 1.1 6.8 1.1 6.8 1.1 6.8 1.1 6.8 1.1 6.8 1.1 6.8 1.1 6.8 1.1 7.8 7.8 7.8 7.8 7.8 7.8 7.8 7.8 7.8 7.8 7.8 7.8 <td>n d</td> <td>2.16</td> <td>1.23</td> <td>1.16</td> <td>0.43</td> <td>1.5</td> <td>9.0</td> <td>0.89</td> <td></td> <td></td> <td>1.16</td> <td></td> <td>0.23</td>	n d	2.16	1.23	1.16	0.43	1.5	9.0	0.89			1.16																0.23
5.3 2 5.8 4.6 5.2 4.7 5.8 4.1 4.8 3.2 7.1 4.8 5.2 7.3 3.4 4.6 4.9 4.0 4.0 4.0 4.0 4.0 4.0 5.2 5.4 4.0 4.0 4.0 4.0 4.0 5.0 4.0	3 £	1.79	0.85	9.34	٩/٠٠	98 0	2.84	9.24			0.82																1.07
1,156	2 6	8.72	5.52	5.33	5 2	5.81	4.06	4.66			5.5																1.67
14. 148 149 2.69 2.66 3.14 2.23 1.29 3.63 2.65 1.81 4.67 2.61 3.02 2.63 0.57 0.57 0.57 0.57 0.57 0.57 0.57 0.57	î 운	1.92	1.2	1.05	0.44	1.34	0.91	-			1.16																0.36
0.51 0.28 0.48 0.48 0.41 1.3 1.3 1.4 0.48 0.42 0.48 0.48 0.48 0.48 0.49 0.49 0.53 0.42 0.55 0.59 0.49 0.51	Ë	5.46	3,46	3.17	1.36	3.99	2,65	3.14			3,63																1.19
3.4 3. 2.8 3.6 3.6 3.6 3.6 3.6 3.6 3.6 3.7 3.2 3.6 3.6 3.6 3.6 3.6 3.7 3.2 3.7 3.2 3.7 3.2 3.7 3.2 3.7 3.2 3.7 3.2 3.7 3.2 3.7 3.2 3.7 3.2 3.7 3.2 3.7 3.2 3.2 3.2 3.2 3.2 3.2 3.2 3.2 3.2 3.2	T.	0.81	0.55	0.51	0.21	0.58	0.46	0.48			0.53																0.18
1.38 0.46 0.45 0.45 0.45 0.45 0.45 0.45 0.45 0.45	Q.	5.18	3.43	3.22	1.39	3.61	2.89	2.98			3.36																1.27
0.07 0.04 0.11 0.07 0.04 0.04 0.04 0.04 0.17 0.12 0.04 0.13 0.05 0.06 0.03 0.14 0.05 0.1 0.03 0.04 0.04 0.05 0.05 0.10 0.05 0.10 0.05 0.1 0.10 0.05 0.1 0.10 0.05 0.1 0.10 0.05 0.1 0.10 0.10	3 %	3.49	0.30	1 78	0.96	1.69	121	1.55			2.58																0.10
NA NA 114 NA 178 0.37 121 0.47 0.48 0.85 1.62 1.73 0.61 0.61 0.62 3.81 2.85 1.7 2.84 0.8 1.7 2.84 0.8 1.45 2.21 2.82 2.05 2.05 0.15 0.15 0.25 0.15 0.15 0.15 0.15 0.15 0.15 0.15 0.1		0.17	0.14	0.07	0.0	0.11	0.07	0.04			0.17																0.03
0.15 0.33 0.27 0.87 0.14 0.13 0.14 0.52 0.25 0.25 0.15 0.15 0.15 0.15 0.15 0.15 0.15 0.1	- Q	Ą	N A	¥	N A	1.14	N A	1.78			0.72																1.38
0.08 0.1 0.17 0.49 0.06 0.1 0.08 0.28 0.18 0.09 0.16 0.07 0.16 0.03 0.18 0.09 0.04 0.07 0.04 0.04 0.07 0.06 0.14 0.21 0.23 0.28 0.08 0.15 0.07 0.04 0.07 0.04 0.02 0.06 0.14 0.21 0.23 0.28 0.08 0.08 0.08 0.08 0.08 0.08 0.08	£	0.42	0.38	0.15	0.33	0.27	0.87	0.11			0.52																0.31
1.00 0.81 0.84 0.67 0.73 0.90 0.63 0.94 0.95 0.64 1.01 0.92 0.92 0.80 1.01 0.67 0.74 0.77 0.75 0.82 0.77 0.76 0.80 0.89 0.89 0.89 0.89 0.89 0.89 0.89	⊃	0,33	0.27	0.08	0.1	0.17	0.49	90.0			0.28																0.16
1.00 0.81 0.84 0.67 0.73 0.90 0.63 0.94 0.95 0.64 1.01 0.82 0.80 1.01 0.87 0.74 0.77 0.76 0.82 0.77 0.76 0.80 0.89 0.89 0.89 0.79 0.80 0.89 0.89 0.89 0.89 0.89 0.89 0.8	ment ratios (N		malized*)																								
0.75 1,15 0,73 0,97 0,94 0,81 0,93 1,07 0,90 0,77 0,92 0,67 1,09 0,54 0,92 0,60 0,88 0,51 0,44 0,54 0,89 0,99 0,99 0,99 0,99 0,99 0,99 0,99	3d/Lu	1.03	0.86	1.00	0.81	0.84	0.67	0.73	0.90	0.63	0.94												0.77	0.76		0.89	0.63
0.85 0.86 0.86 0.89 0.89 0.89 0.89 0.81 0.88 0.89 0.81 1.02 0.81 1.02 0.81 1.01 0.86 0.89 0.83 0.89 0.83 0.86 0.89 0.83 1.00 (2012)	a/Sm	0.95	0.81	0.75	1.15	0.73	0.97	0.64	0.81	0.93	1.07												0.58	0.69		0.1	1.52
[2012]	-a/Lu	1.00	0.72	0.63	0.79	0.55	0.50	0.39	69.0	0.49	1.02												0.39	0.47		0.85	0.88
B nomizitation values from Gale et al. (2012)		3	3	3	2	3	2		2	2	2												3			3	5
	B normalizatio,	n values fror	n Gale et al.	(2012)																							

BECKER ET AL. 9 of 20

15252027, 2024, 7, Downloaded from https://agupubs.onlinebtrary.witey.comdoi/10.1029/2023GC011412 by Dainl Viete - Johns Hopkins University , Wiley Online Library on [1107/2024] See the Terms and Conditions (https://onlinelibrary

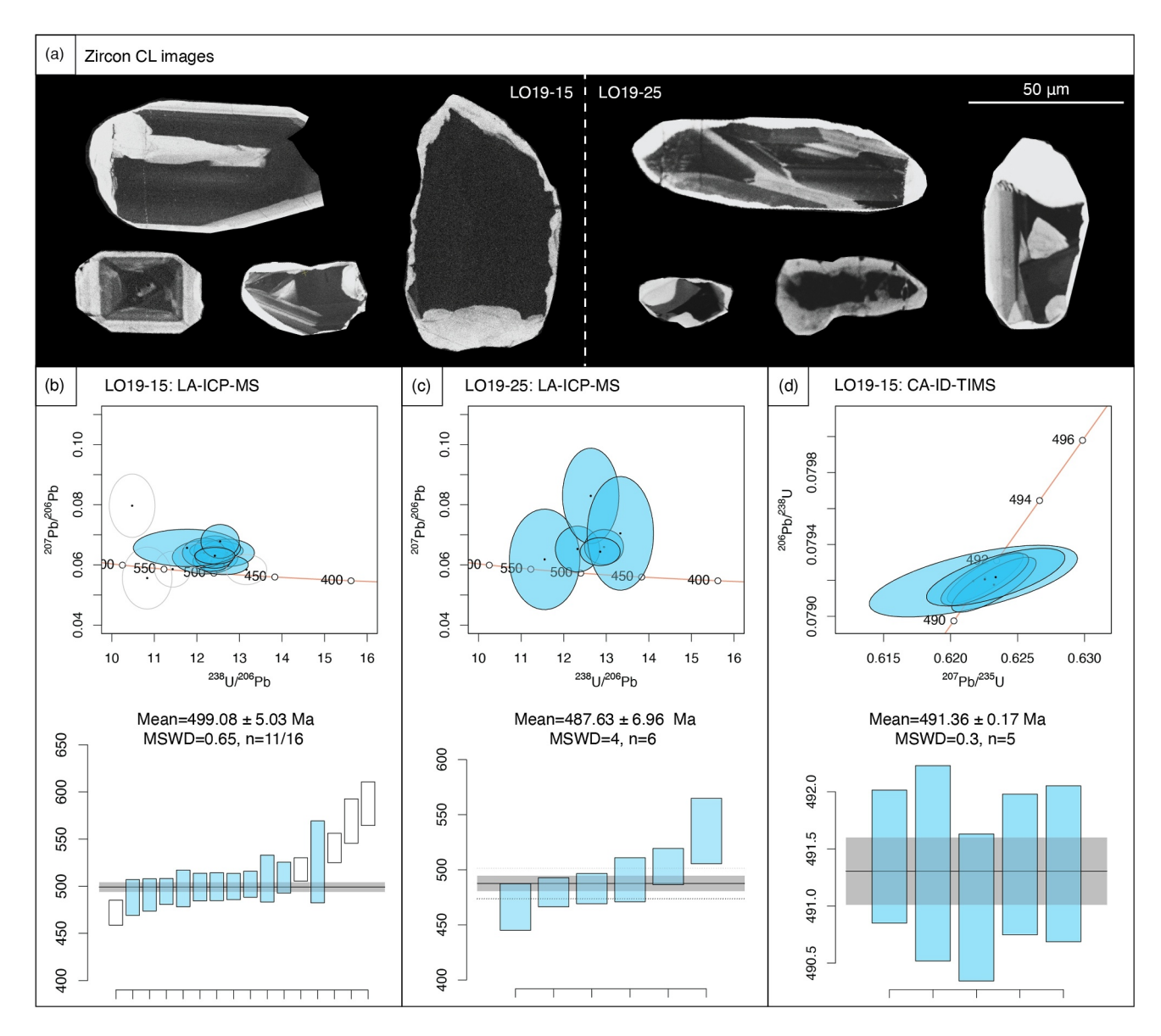


Figure 4. (a) Cathodoluminescence images of representative zircons from sample LO19-15 and sample LO19-25; Tera-Wasserburg diagrams and weighted mean age plots for LA-ICP-MS analyses of sample (b) LO19-15 and (c) sample LO19-25; (d) Wetherill diagram and weighted mean age plot for CA-ID-TIMS analyses of sample LO19-15. Uncertainties are 2s (sample standard deviation) for LA-ICP-MS dates and 95% confidence for CA-ID-TIMS date.

3.5. Geochronology

Two amphibolite samples—LO19-15 and LO19-25—yielded sufficient zircon for U-Pb geochronology. LO19-15 was collected from the southern tip of Leka (Figure 1b) and is geochemically similar to IBM FAB. Zircons (n=16) were 20–100 μ m in length, euhedral to subhedral, and displayed oscillatory, sector, or patchy zoning in CL (Figure 4a). U-Pb zircon analyses by LA-ICP-MS for LO19-15 define a single population (MSWD = 0.65, n=11/16), yielding a weighted mean 206 Pb/ 238 Pb date of 499.08 \pm 5.03 Ma (Figure 4b). Th/U is 0.41–1.26.

LO19-25, collected approximately 10 km to the NE of LO19-15 (Figure 1b), is also geochemically consistent with IBM FAB. Zircons (n = 6) were 20–100 µm in length, euhedral to subhedral, and displayed patchy zoning, darker cores, and lighter rims in CL (Figure 4a). U–Pb zircon analyses by LA-ICP-MS for LO19-25 are overdispersed relative to what may be expected for a single population (MSWD = 4, n = 6), yielding a weighted mean $^{206}\text{Pb}/^{238}\text{Pb}$ date of 487.63 \pm 6.96 Ma (Figure 4c). Th/U is 0.27–0.72.

BECKER ET AL. 10 of 20

Five LA-ICP-MS-analyzed zircon grains from sample LO19-15 were selected for CA-ID-TIMS analysis, yielding a weighted mean 206 Pb/ 238 U date (Figure 4d) of 491.36 \pm 0.17|0.22|0.56 Ma (randomltracer included) decay constant included). The CA-ID-TIMS analyses show a distribution consistent with a single population (MSWD = 0.3, n = 5) and the Th/U is 0.235–0.697.

4. Discussion

4.1. The IBM Model of Tectonomagmatic Discrimination

A detailed record of tectonomagmatic processes in an active subduction zone have been documented through extensive investigations of the magmatic products preserved in the IBM forearc (Arculus et al., 2015; Bryant et al., 2003; Ishizuka et al., 2011; Li et al., 2021; Pearce & Reagan, 2019; Pearce et al., 2015; Reagan et al., 2010, 2019; Shervais et al., 2019, 2021; Stern et al., 2012; Whattam & Stern, 2011). Mafic units sampled from the base of the IBM forearc magmatic stratigraphy display geochemistry consistent with formation from decompression melting resulting from intense forearc extension as the oceanic lithosphere began to founder. The high degrees of partial melting produced forearc basalts (FAB) with geochemistry similar to mid-ocean ridge basalts (MORB) but distinguished by differences in high field strength element (HFSE) and heavy rare earth element (HREE) concentrations (Reagan et al., 2010; Shervais et al., 2019).

FAB melt extraction left the residual mantle depleted in incompatible elements (Reagan et al., 2010). As subduction was established, volatiles released from the subducting slab resulted in flux melting of the depleted mantle wedge and the generation of immobile element-depleted, fluid mobile element-enriched boninitic (BON) melts (Reagan et al., 2010). Records of this geochemical evolution are preserved spatially as BON overlying FAB in the IBM forearc magmatic stratigraphy (Reagan et al., 2010).

U-Pb zircon crystallization dates on IBM gabbros indicate that seafloor spreading began nearly simultaneously (51.94 \pm 0.13 Ma and 51.81 \pm 0.03 Ma, respectively) 1700 km apart in the Bonin and Mariana forearcs (Reagan et al., 2019). Geochemical evolution in the IBM forearc is constrained to less than 1 million years by 40 Ar/ 39 Ar ages on volcanic glass and pyroxenes that record decompression melting and FAB magmatism at 51.34 \pm 0.78 Ma, followed by flux-associated melting and BON magmatism at 51.27 \pm 0.09 Ma to 50.33 \pm 0.55 Ma (Reagan et al., 2019). FAB erupted close to the trench, but the moved away from the trench as seafloor spreading progressed (Reagan et al., 2019). In contrast, BON erupted close to the spreading center and migrated toward the trench as the subduction zone became established, resulting in lateral (trench and forearc perpendicular) spatial variation in the IBM forearc magmatic stratigraphy (Reagan et al., 2019).

The IBM model has been used to evaluate potential subduction zone forearc origins for SSZ ophiolites (Ishizuka et al., 2011; Reagan et al., 2010). The Neotethyan Samail Ophiolite shows similar geochemical progression and timescales for magmatic evolution from FAB to BON in <1–2 million years (Dilek & Furnes, 2009; Dilek et al., 2007, 2008; Godard et al., 2003; Ishikawa et al., 2002; Kusano et al., 2017; Reagan et al., 2010; Rioux et al., 2021; Shervais, 2001) which suggests that it too may represent forearc lithosphere formed during subduction initiation (Shafaii Moghadam et al., 2013). The Samail Ophiolite and SSZ ophiolites of similar age within the regionally extensive Alpine–Zagros–Himalayan Mountain system may have formed rapidly along a vast sector of the Neotethys Ocean, analogous to the IBM (Shafaii Moghadam et al., 2013). The apparent rapid tectonomagmatic evolution recorded by the FAB-to-BON succession in the IBM forearc and Neotethyan SSZ ophiolites indicates that crystallization ages obtained on FAB units can be utilized to determine the approximate timing of subduction initiation along 1,000s km of strike, providing valuable insights into the kinematics associated with new plate boundary development.

4.2. Effects of Metamorphism on Tectonomagmatic Discrimination Schemes

The tectonomagmatic classification approach developed for the IBM system relies on major and trace element discrimination schemes that were developed on lavas, shallow microgabbroic intrusions, and gabbros collected from dredging and drilling in the IBM forearc. These units remained in the near-surface environment and experienced limited degrees of post-magmatic, high-temperature metamorphism. Consequently, when applying the IBM classifications to ophiolites that have undergone significant post-magmatic tectonism, it is essential to assess whether elemental mobilization associated with secondary alteration has occurred. Below, the potential effects of post-magmatic element mobility are assessed and IBM-based tectonomagmatic classifications are

BECKER ET AL. 11 of 20

considered with emphasis on "seeing through" the potential influences of metamorphism and metasomatism to identify signatures that can confidently be linked to primary tectonomagmatic processes.

Linear correlations between elements considered immobile during high-temperature metamorphism (Y, Yb, Nb, Zr) are used to determine the most immobile element in the sample suite (method outlined in Guice et al., 2018, 2019). For the LOC samples, Y and Yb have a strong linear correlation ($R^2 = 0.99$), indicating minimal relative fractionation due to secondary alteration. This is further supported by the poor correlations between Y and the fluid-mobile large-ion lithophile elements (LILE; Ba, Cs, Rb, Sr), which yield R^2 values ≤ 0.042 . Comparison of analyzed trace elements to the immobile element Y determines which elements are likely to have experienced secondary post-crystallization mobilization (Figure S1 in Supporting Information S1). The high field strength elements (HFSE; Nb, Zr, Hf, Ta) all show moderate correlation with Y ($R^2 \geq 0.58$), indicating limited secondary mobilization of these elements. The strongest correlations are between the light rare earth elements (LREE) and Y ($R^2 \geq 0.70$) and the heavy rare earth elements (HREE) and Y ($R^2 \geq 0.97$). Ti and V are often used as proxies for mantle oxidation related to subduction zone fluids. In the LOC samples, Ti has a strong correlation with Y ($R^2 = 0.86$); however, V has only a moderate correlation with Y ($R^2 = 0.40$), indicating likely secondary mobilization and that care must be taken when using it as a discriminator. The results of element mobility analysis indicate that HFSE and REE compositions are the most reliable bulk-rock discriminators for investigating the tectonomagmatic origins of the LOC, and that Ti may also be of use.

4.3. Geochemical Classification of the LOC Rocks

Of the four LOC samples with $TiO_2 < 0.5$ wt.%, two have MgO > 8 wt.% and $SiO_2 \ge 52$ wt.% classifying them as boninites (BON) according to the IUGS classification as well as the Ti8 versus Si8 boninite classification diagram (Figure 6a) of Pearce and Reagan (2019). The other two samples are classified as low-Ti basalts (LoTi), which are considered altered boninites that have undergone Mg and Si loss via secondary alteration (Pearce & Reagan, 2019).

The remaining LOC samples have $TiO_2 > 0.5$ wt.%, SiO_2 of 49.14-55.59 wt.%, and MgO 4.48-10.18 wt.% (Figures 5b and 5c), overlapping with IBM FAB and IBM HMA on major element classification diagrams (Pearce & Reagan, 2019). Further discrimination using Yb versus Ce/Yb (Shervais et al., 2019) classifies nine LOC samples as normal FAB (N-FAB), with Ce/Yb = 1.0-2.0 and Yb = 2.0-4.5 ppm consistent with IBM N-FAB (Figure 5d). The remaining LOC samples have mixed affinities between IBM N-FAB and enriched-FAB (E-FAB); their Ce/Yb range overlaps with IBM E-FAB (Ce/Yb = 2.2-3.8) but extends to higher values than IBM E-FAB, whereas their Yb contents (Yb = 2.14-5.18 ppm) more closely align with values for IBM N-FAB than IBM E-FAB. These samples are classified as E-FAB based on their Ce/Yb ratios.

The four classes of LOC samples defined above (BON, LoTi, N-FAB, E-FAB) show consistent signatures within each group when plotted on common basaltic discrimination diagrams. The LOC BON and LoTi have low Ti/V ratios (Ti/V < 10) but with higher concentrations of V than IBM BON (Figure 5e); this is likely the result of secondary V mobilization, as discussed in Section 4.1. The N-FAB and E-FAB samples plot along the dividing line between island-arc tholeites (IAT) and mid-ocean ridge basalt (MORB) at Ti/V = 20 with three E-FAB samples at higher Ti concentrations and one N-FAB sample plotting at low Ti concentrations but with V concentrations significantly higher than the BON and LoTi groups (Figure 5e). The LOC samples plot entirely along the MORB dividing line and within the oceanic arc field on the Nb_N versus Th_N discrimination diagram (Figure 5f; Saccani, 2015). The samples with Th_N elevated over the IBM values may have experienced secondary Th mobilization, as discussed in Section 4.1.

Chondrite-normalized REE diagrams and N-MORB-normalized extended trace element diagrams show similarities among the samples assigned BON and LoTi classifications based on major and trace elements; all show depleted REE concentrations, Ta-Nb and Hf-Zr depletions, and LILE (Rb, Ba, Sr), Th and U enrichment relative to N-MORB (Figures 6a and 6b). Overall, the BON and LoTi patterns match closely with that of average IBM BON, but with higher concentrations of HREE. The N-FAB and E-FAB REE geochemistry are similar, with REE patterns showing LREE depletion relative to HREE; however, the total REE concentrations of E-FAB samples are higher than those of N-MORB and average IBM FAB. Some samples show Ta-Nb depletions of similar scale to the BON and LoTi samples, but Hf-Zr and REE depletions align more closely with IBM FAB. Some E-FAB samples can be distinguished on the basis of a negative Sr anomaly that is not seen in any other LOC

BECKER ET AL. 12 of 20

wiley.com/doi/10.1029/2023GC011412 by Daniel Viete - Johns Hopkins University, Wiley Online Library on [11/07/2024]. See the Terms and Conditions (https://www.doi.org/10.1029/2023GC011412).

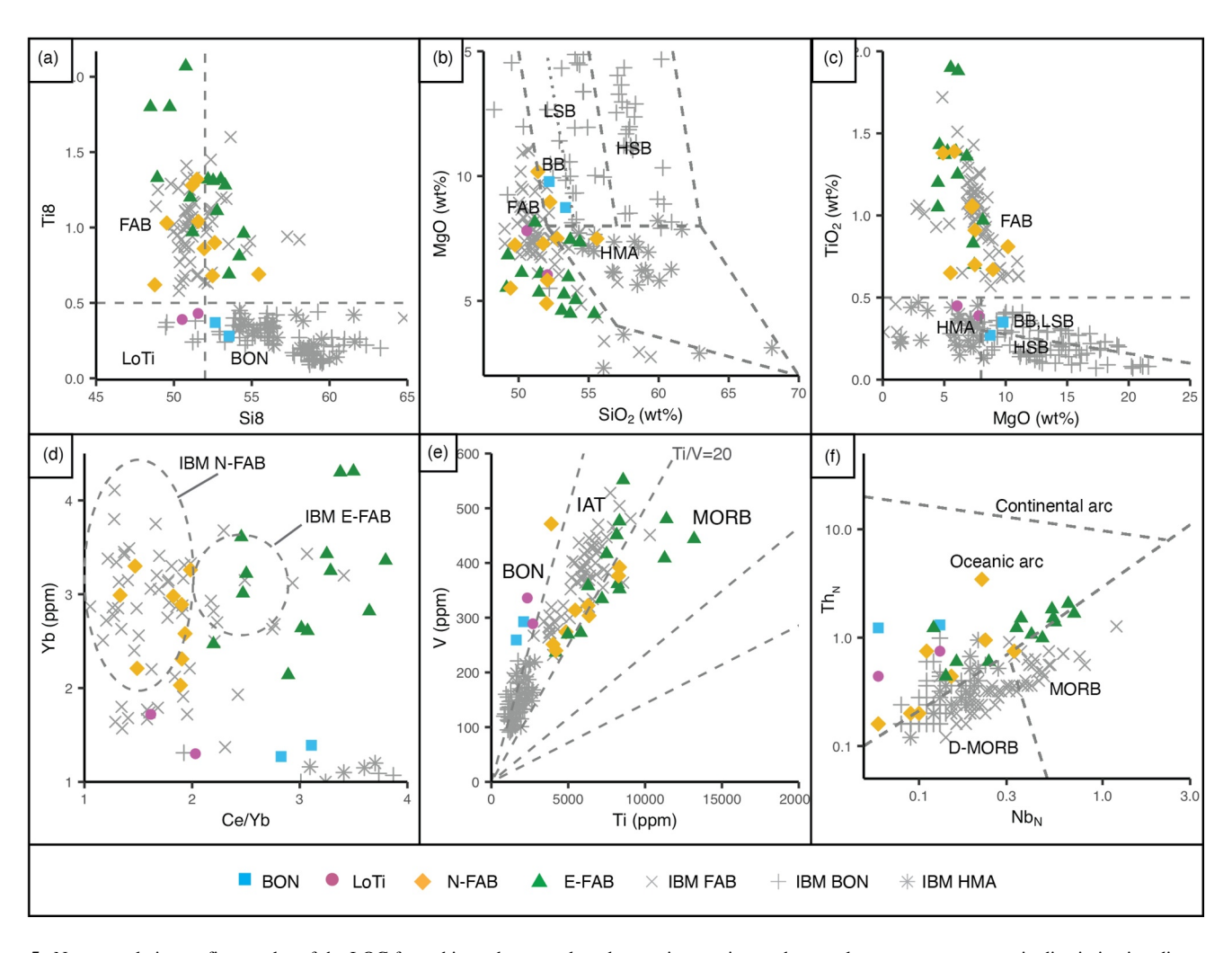


Figure 5. Non-cumulative mafic samples of the LOC from this study were plotted on various major- and trace-element tectonomagmatic discrimination diagrams. Geochemical classifications based on the IBM model include: (a) Ti8 versus Si8 boninite discrimination diagram (after Pearce & Reagan, 2019); (b) MgO versus SiO₂ bivariate diagram (after Pearce & Reagan, 2019), and (d) Yb versus Ce/Yb plot for FAB discrimination (after Shervais et al., 2019). (e) Ti versus V oceanic basalt classification diagram (after Shervais, 1982). (f) Normalized Th versus Nb tectonic classification diagram (after Saccani, 2015). N-MORB normalizing values are from Gale et al. (2012). Literature IBM data are from Ishizuka et al. (2011), Pearce and Reagan (2019), Reagan et al. (2010, 2019), and Shervais et al. (2021). Abbreviations: BB = basaltic boninite; BON = boninite; D-MORB = depleted-MORB; E-FAB = enriched FAB; FAB = forearc basalt; HMA = high-magnesium andesite; HSB = high-silica boninite; IAT = island arc tholeiite; IBM = Izu-Bonin-Mariana; LoTi = low-titanium basalt; LSB = low-silica boninite; MORB = mid-ocean ridge basalt; N-FAB = normal FAB.

samples; when combined with a minor negative Eu anomaly, the Sr depletion may indicate extraction from a source that underwent minor plagioclase loss as a result of crystal fractionation.

4.4. Geochronology of the LOC Rocks

The 491.36 ± 0.17 Ma date on LO19-15 is interpreted to record the igneous crystallization of Leka FAB units. We note that the CA-ID-TIMs and LA-ICP-MS dates for LO19-15 are different within uncertainty, likely reflecting unaccounted for inaccuracy in the LA-ICP-MS approach (Schaltegger et al., 2015). The zircons in LO19-15 are interpreted to be igneous in origin. Geochemical similarity of LO19-15 to IBM FAB samples suggests that the 491.36 ± 0.17 Ma date for LOC records magmatic activity during the earliest stages of subduction initiation, prior to arc development. Our new CA-ID-TIMS data suggest that a previously published U-Pb zircon date $(497 \pm 2 \text{ Ma}; \text{Dunning \& Pedersen}, 1988)$ that was considered to capture the timing of LOC formation may have been an overestimate. Overdispersion in the LA-ICP-MS data for sample LO19-25 may reflect metamorphic/metasomatic zircon overgrowth and/or Pb uptake/loss within the outer parts of the zircon grains.

BECKER ET AL. 13 of 20

15252027, 2024, 7, Downloaded from https://agupubs.onlinelibrary.wiley.com/doi/10.1029/2023GC011412 by Daniel Viete - Johns Hopkins University, Wiley Online Library on [11/07/2024]. See the Terms and Conditions (https://

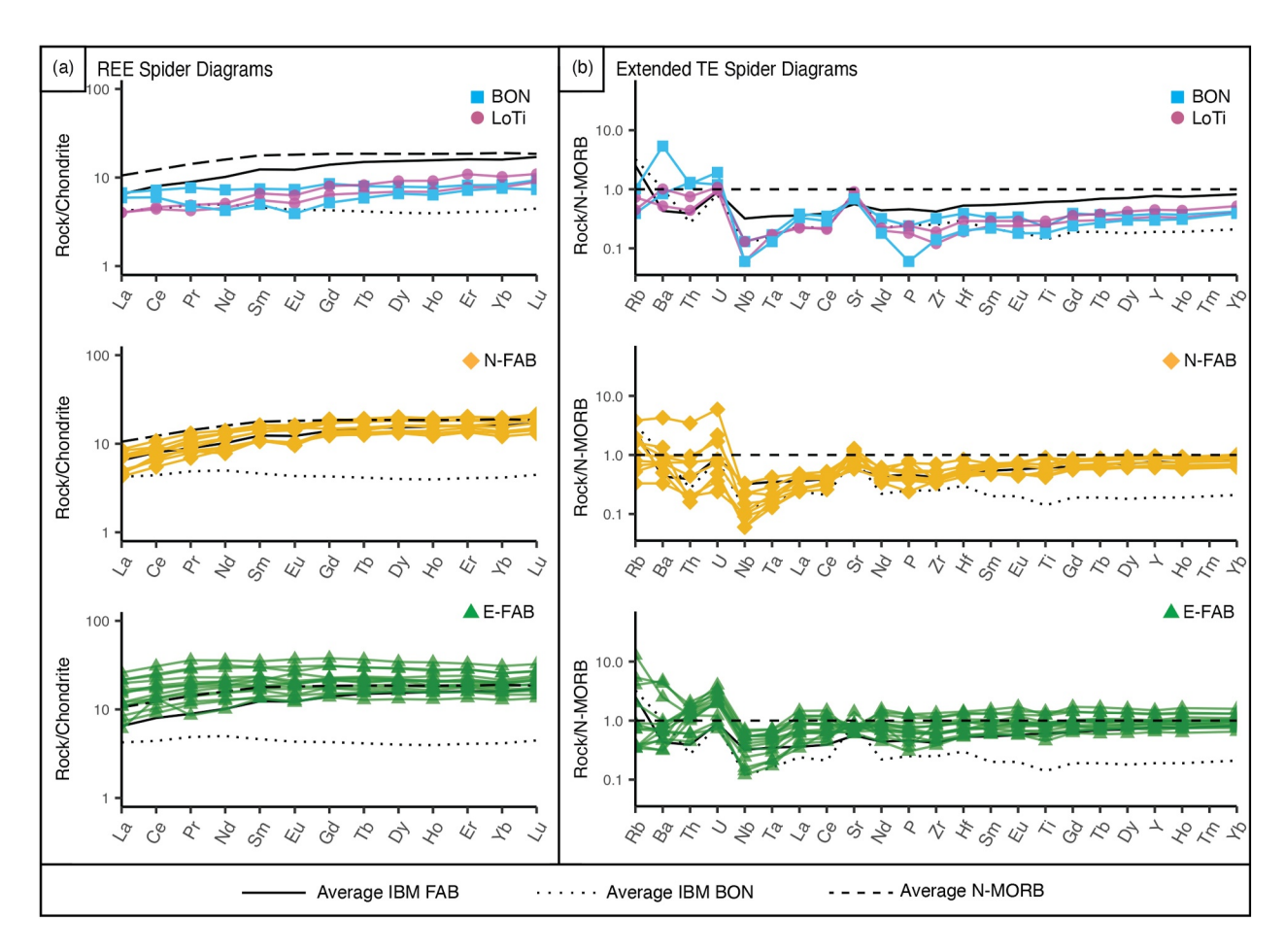


Figure 6. Rare earth element (REE) and extended trace element (TE) spider diagrams for the non-cumulate samples of the LOC. (a) Chondrite-normalized REE spider diagram with LOC samples compared to average forearc basalt (FAB) and boninite (BON) compositions for the IBM forearc. (b) N-MORB-normalized extended trace element spider diagram with LOC samples compared to average IBM FAB and IBM BON compositions. IBM FAB and BON averages calculated from Ishizuka et al. (2011), Pearce and Reagan (2019), Reagan et al. (2010, 2019), and Shervais et al. (2021). Chondrite normalizing values are from Barrat et al. (2012) and N-MORB normalizing values are from Gale et al. (2012).

4.5. Spatial Distribution of Lava Types in the LOC

The LOC pseudostratigraphy indicates that southern Leka, which is situated closer to the LOC mantle section, represents deeper levels of the magmatic stratigraphy than on Madsøya. This implies that the units on Leka may be the oldest among the sampled areas of non-cumulate rocks (Figure 7a). One sample from the island of Leka is N-FAB (Figure 7b) and the remainder are E-FAB (Figure 7a), whereas Madsøya yielded equal amounts of E-FAB and N-FAB samples (Figure 7b). The E-FAB and N-FAB units are dispersed across Madsøya, with the greatest number of N-FAB units located on the southernmost portion of the islet (Figure 7b). The LOC BON and LoTi are only present on the islets of Madsøya and Frøvikøya (Figure 7b). The presence of BON and LoTi units as well as the occurrence of pillow basalts on Madsøya (Figure 1h) supports the interpretation that the islet represents higher levels of the LOC pseudostratigraphy than Leka. Units within the LOC gabbro section on Leka are dominantly E-FAB, suggesting that they may have formed earlier than the N-FAB units on Madsøya. This interpretation is reinforced by their comparatively less-depleted HFSE and REE concentrations as well as lower concentrations of LILE in most of the E-FAB samples. Notably, three E-FAB samples exhibit significantly higher LILE concentrations (LO22-06B, LO22-47, LO22-44); these samples also exhibit high concentrations of K, contain biotite, and are in the uppermost portion of the LOC pseudostratigraphy, suggesting that the high LILE concentrations may originate from interaction with sediments.

BECKER ET AL. 14 of 20

15252027, 2024, 7, Downloaded from https://agupubs.onlinelibrary.wiley.com/doi/10.1029/2023GC011412 by Daniel Viete - Johns Hopkins University, Wiley Online Library on [11/07/2024]. See the Terms and Condition

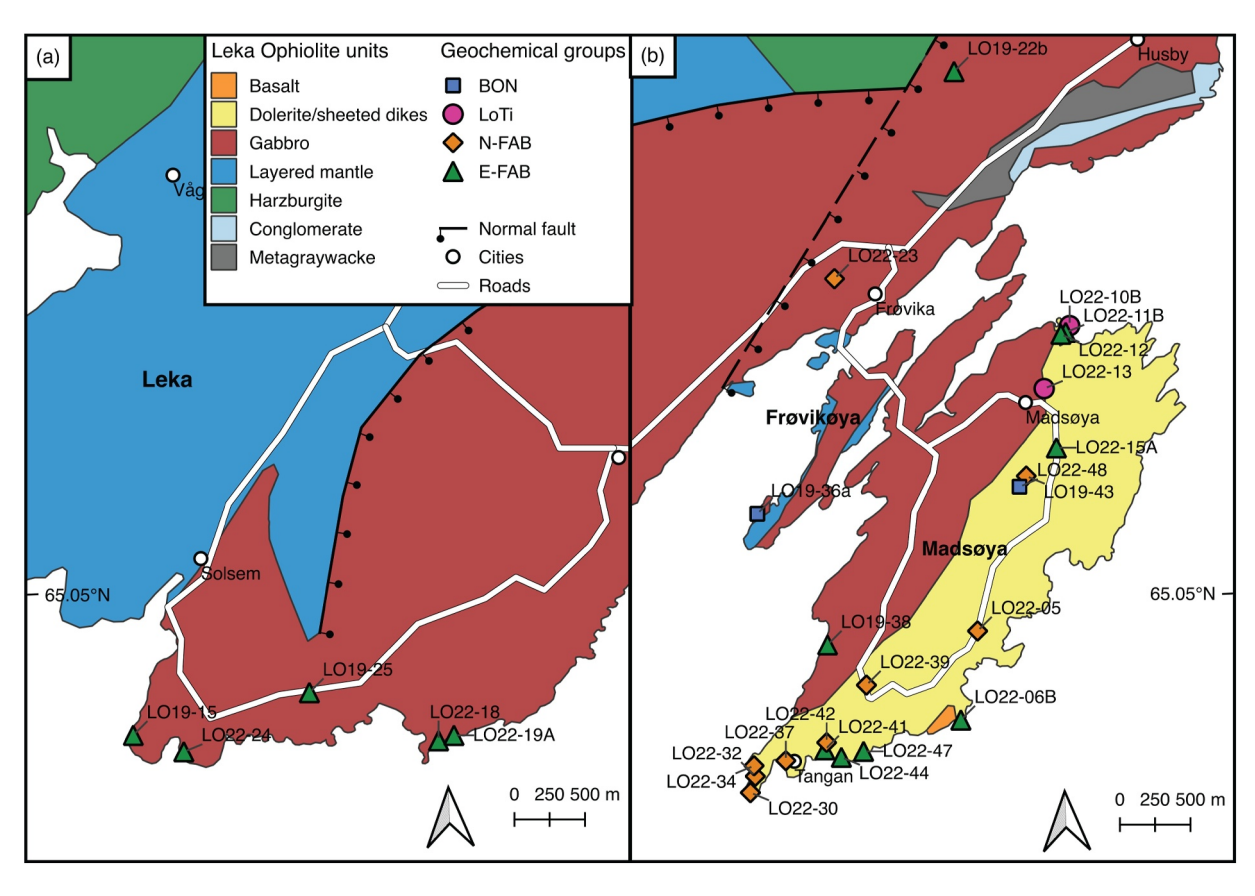


Figure 7. Maps of southwestern Leka and of the island of Madsøya with samples plotted by geochemical classification. (a) E-FAB samples on southwest Leka. (b) LOC samples on western Leka, Frøvikøya, and Madsøya. Inset in (a) also applies to (b). Abbreviations: BON = boninite; E-FAB = enriched forearc basalt; N-FAB = normal forearc basalt; LoTi = low-titanium boninite.

4.6. Connecting Phase, Process, and Product in SSZ Ophiolites

Ophiolites preserve only a partial record of their formation environment. Hence, their origins must be deduced from the magmatic products they preserve, what process those products represent, and to which tectonic phase that process belongs. Figure 8 illustrates forearc lithosphere development and the connection between phase, process, and products. In the "Initiating" phase of subduction, the dominant magma genesis process is mantle decompression melting due to slab sinking, extension in the forearc region, and seafloor spreading. This process produces forearc basalts as the first magmatic product of subduction. The second tectonic phase outlines a "Developing" subduction system in which the sinking slab begins to release volatiles and fluids into the previously depleted mantle from which the forearc basalts were extracted. The primary magma genesis process during this phase is flux melting to produce incompatible element-depleted fluid mobile element-enriched boninites. The final tectonic phase is one of a "Developed" arc (i.e., protoarc development), which is facilitated by steady-state subduction and mantle wedge recharge to produce typical island arc volcanics.

In Figure 8, example cross sections from various locations across the Phase 3 ("Developed") forearc are shown to illustrate spatial variability across the forearc; three distinct schematic sections are shown perpendicular to the spreading axis. The first column (a) shows a section on the trench-distal side of the spreading center, which is dominated by early FAB with only minor amounts of BON recorded. The LOC is representative of this section. The second column (b) is taken from the center of the forearc and includes early FAB overlain by BON and a thick layer of island arc volcanics. An example of an Appalachian–Caledonian ophiolite matching this section may be the Baltimore Mafic Complex of Maryland, USA (Guice et al., 2021; Hanan & Sinha, 1989). The third column (c) is taken from the trench-proximal side of the spreading center and is dominated by BON, with only minor amounts of FAB. The Thetford Mines Ophiolite of Quebec, Canada, is an example of an Appalachian–Caledonian ophiolite with a BON-dominated magmatic stratigraphy (Laurent & Hébert, 1989; Olive et al., 1997).

BECKER ET AL. 15 of 20

15252072, 2024, 7, Dowloaded from https://gupubs-onlinebitary.wiley.com/doi/1.0109/2023GC011412 by Daiel Viete - Johns Hopkins University, Wiley Online Library on [1107/2024] See the Terms and Conditions (https://onlinebitary.wiley.com/terms-and-conditions) on Wiley Online Library for rules of use; OA articles are

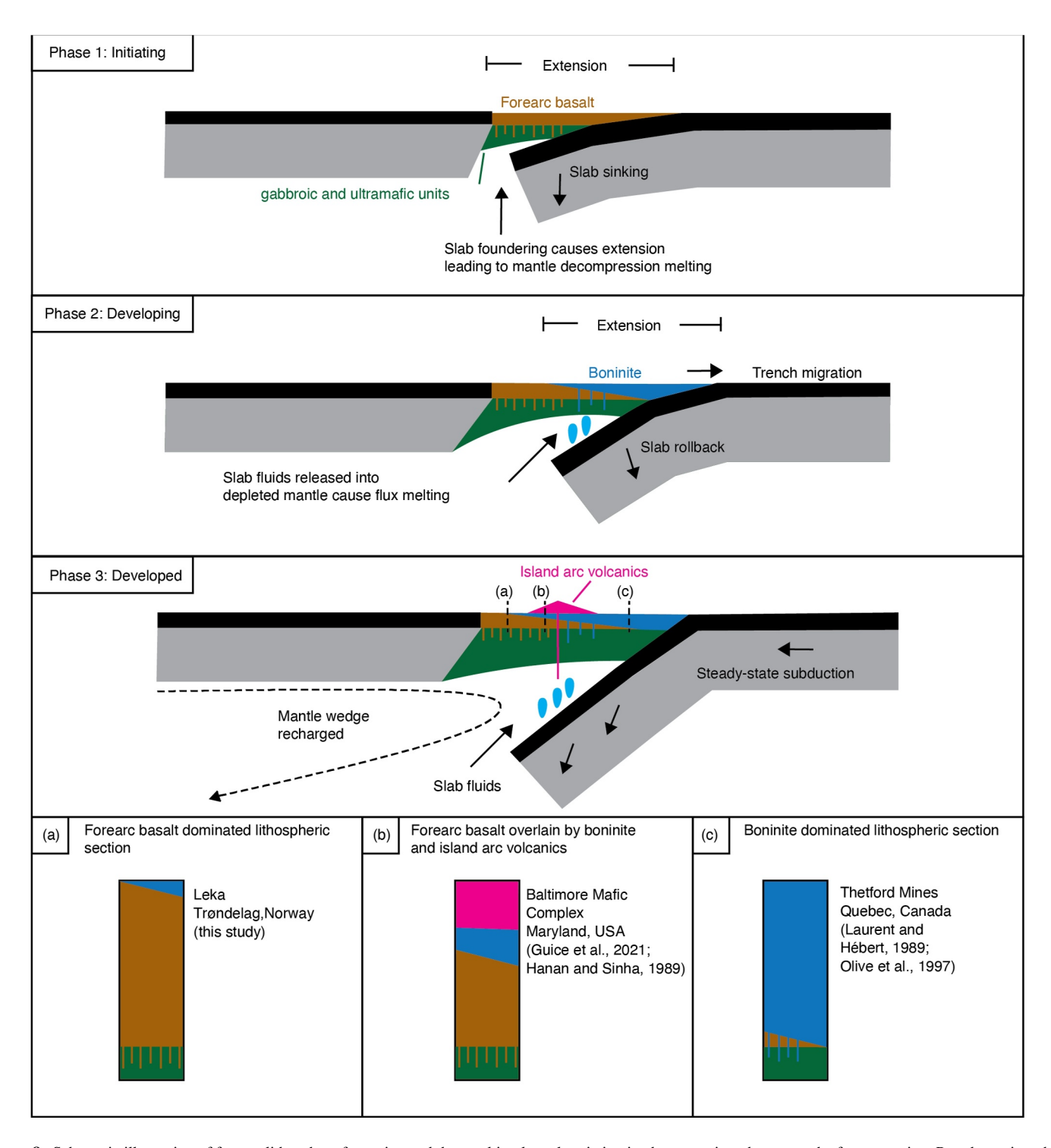


Figure 8. Schematic illustration of forearc lithosphere formation and the resulting lateral variation in chemostratigraphy across the forearc region. Pseudostratigraphic columns demonstrate forearc variability that is sampled by/preserved in the magmatic sequences of select Appalachian–Caledonian ophiolites. See text for discussion.

4.7. The Origin and Preservation of the Leka Ophiolite Complex

The LOC preserves mafic units with both FAB and BON geochemistries, with FAB being the dominant type. The association of these two geochemical types suggests that the LOC primarily records the early stages of forearc extension and decompression melting but retains little evidence of the latter phases of subduction evolution and development of a volcanic arc. This truncated record (compared to the complete record preserved across the IBM

BECKER ET AL. 16 of 20

15252027, 2024, 7, Downloaded

Acknowledgments

The authors thank Val Finlayson for the

beneficial review that improved the final manuscript. The authors also wish to

express their gratitude to Dana Brenner for

analysis, Stanley Mertzman for assistance with whole-rock XRF analysis, and Anna

Burkholder and Emma Penafiel for their

assistance with sample processing. We also thank the owners and hosts of Leka

Motell og Camping, Anne Britt Normann and Jostein Hiller, for their hospitality and

guidance during the fieldwork. Calvin Barnes, Melanie Barnes, and Aaron

Yoshinobu from Texas Tech University

are thanked for sharing their knowledge during a chance encounter in the field on Leka. Funding for this project was provided by National Science Foundation

(NSF) CAREER Grant (NSF-2042631),

NSF Infrastructure and Facilities Grant

(NSF-1831766), JHU Catalyst Grant,

Hopkins Extreme Materials Institute Seed Grant, two JHU Department of Earth and

Planetary Sciences Field Research Grants.

Lewis and Clark Fund for Exploration and

and an American Philosophical Society

Field Research Grant

assistance with whole-rock LA-ICP-MS

forearc) may result from spatial variations in the SSZ lithosphere associated with trench migration and lateral movement of magmatism. In this scenario, the LOC may represent a forearc section that underwent only very minor slab fluid involvement as the initial FAB magmatism moved away from the forearc spreading center. The original subduction forearc system may have been expansive, yet only a small portion of the early FAB-dominated record is now preserved as the LOC.

The LOC may also represent a short-lived episode of extension that ended prior to development of a mature subduction zone. FAB magmatism in the IBM lasted 1–2 Myr before transitioning to BON and more evolved arc magmatism (Reagan et al., 2019); therefore, if forearc system development associated with the LOC ceased within this timeframe, no evolved arc lava would have been produced. If subduction initiation occurred in a narrow oceanic tract, closure of the tract would have occurred soon after subduction initiation as the oceanic lithosphere was consumed, terminating subduction prior to substantial arc development. This setting could also favor ophiolite preservation due to the proximity of the young and buoyant forearc lithosphere to the continent. The less oxidized nature of the LOC mantle portion, compared to what is typically expected in a mature subduction zone (O'Driscoll et al., 2021), supports the hypothesis that the LOC formed in association with a short-lived (and/or early stage) subduction zone.

The variation between IBM FAB and LOC FAB may also originate from their respective mantle sources. The IBM shows evidence of an extremely depleted mantle source potentially related to extraction from the previously depleted Indian Ocean mantle; therefore, the IBM forearc may reflect greater depletion in incompatible elements than forearc lithosphere from other subduction zones (Shervais et al., 2019). In contrast, LOC FAB units are less depleted in incompatible elements, suggesting extraction from a less depleted mantle source.

The LOC context and history undoubtedly affect which forearc lithosphere segments are now exposed and preserved. Within the LOC pseudostratigraphy, tens of km of crustal section is presumed missing in the region of a major NE–SW normal fault that juxtaposed upper crustal rocks (mapped gabbro unit) with layered mantle section rocks. Other LOC segments may have been buried, removed, or eroded during subsequent tectonic events. The specific formation, obduction, deformation, and uplift/erosion history of the LOC all had an influence over which parts of a presumably much more extensive and magmatically diverse forearc region (Figure 8) are ultimately sampled and preserved.

5. Conclusions

- The LOC preserves a record of geochemical variation from forearc basaltic to boninitic magmatism, reflecting formation during initiation and early evolution of a subduction zone.
- A 491.36 ± 0.17 Ma U-Pb zircon date for a forearc basalt unit in the LOC is considered to date subduction initiation in the "Leka sector" of the Iapetus Ocean.
- Differences between the LOC and the model IBM forearc pseudostratigraphy may result from selective preservation of a spatially variable forearc lithosphere in addition to the specific history of formation, obduction, deformation, and uplift/erosion of the LOC.
- Other Cambro-Ordovician SSZ ophiolites of the Appalachian—Caledonian system vary in character from the LOC (and from each other), reflecting different contexts of formation within the subduction zone forearc and/ or different post-formation histories.

Data Availability Statement

All data referenced in this paper are available online through the Johns Hopkins Research Data Repository via Becker et al. (2023).

References

Albrektsen, B. A., Furnes, H., & Pedersen, R. B. (1991). Formation of dunites in mantle tectonites, Leka Ophiolite complex, Norway. *Journal of Geodynamics*, 13(3–4), 205–220. https://doi.org/10.1016/0264-3707(91)90039-H

Andò, S. (2020). Gravimetric separation of heavy minerals in sediments and rocks. *Minerals*, 10(3), 273. https://doi.org/10.3390/min10030273 Andresen, A. (1988). Caledonian terranes of northern Norway and their characteristics. *Trabajos sw Geologis*, 17, 103–117.

Arculus, R. J., Ishizuka, O., Bogus, K. A., Gurnis, M., Hickey-Vargas, R., Aljahdali, M. H., et al. (2015). A record of spontaneous subduction initiation in the Izu-Bonin-Mariana arc. *Nature Geoscience*, 8(9), 728–733. https://doi.org/10.1038/ngeo2515

Barrat, J. A., Zanda, B., Moynier, F., Bollinger, C., Liorzou, C., & Bayon, G. (2012). Geochemistry of CI chondrites: Major and trace elements, and Cu and Zn Isotopes. *Geochimica et Cosmochimica Acta*, 83, 79–92. https://doi.org/10.1016/j.gca.2011.12.011

BECKER ET AL. 17 of 20

15252027, 2024, 7, Downloadec

- Becker, N. A., Nelson, W. R., Browning-Hanson, J. F., Crowley, J. L., & Viete, D. R. (2023). Data associated with the publication: Iapetan subduction initiation recorded in the Leka Ophiolite Complex, Norway [Dataset]. Johns Hopkins Research Data Repository, V1. https://doi.org/10.7281/T1/XFNORD
- Bird, J. M., Dewey, J. F., & Kidd, W. S. F. (1971). Proto-Atlantic oceanic crust and mantle: Appalachian/Caledonian ophiolites. *Nature; Physical Science*, 231(19), 28–31. https://doi.org/10.1038/PHYSCI231028A0
- Black, L. P., Kamo, S. L., Allen, C. M., Davis, D. W., Aleinikoff, J. N., Valley, J. W., et al. (2004). Improved ²⁰⁶Pb/²³⁸U microprobe geochronology by the monitoring of a trace-element-related matrix effect; SHRIMP, ID-TIMS, ELA-ICP-MS and oxygen isotope documentation for a series of zircon standards. *Chemical Geology*, 205(1—2), 115–140. https://doi.org/10.1016/j.chemgeo.2004.01.003
- Bryant, C. J., Arculus, R. J., & Eggins, S. M. (2003). The geochemical evolution of the Izu-Bonin arc system: A perspective from tephras recovered by deep-sea drilling. *Geochemistry, Geophysics, Geosystems*, 4(11). https://doi.org/10.1029/2002GC000427
- Crowley, J. L., Schoene, B., & Bowring, S. A. (2007). U-Pb dating of zircon in the Bishop Tuff at the millennial scale. *Geology*, 35(12), 1123–1126. https://doi.org/10.1130/g24017a.1
- Dilek, Y., & Furnes, H. (2009). Structure and geochemistry of Tethyan ophiolites and their petrogenesis in subduction rollback systems. *Lithos*, 113(1–2), 1–20. https://doi.org/10.1016/j.lithos.2009.04.022
- Dilek, Y., & Furnes, H. (2011). Ophiolite genesis and global tectonics: Geochemical and tectonic fingerprinting of ancient oceanic lithosphere. Geological Society of America Bulletin, 123(3–4), 387–411. https://doi.org/10.1130/B30446.1
- Dilek, Y., Furnes, H., & Shallo, M. (2007). Suprasubduction zone ophiolite formation along the periphery of Mesozoic Gondwana. Gondwana Research, 11(4), 453–475. https://doi.org/10.1016/j.gr.2007.01.005
- Dilek, Y., Furnes, H., & Shallo, M. (2008). Geochemistry of the Jurassic Mirdita Ophiolite (Albania) and the MORB to SSZ evolution of a marginal basin oceanic crust. *Lithos*, 100(1–4), 174–209. https://doi.org/10.1016/j.lithos.2007.06.026
- Dunning, G. R., & Pedersen, R. B. (1988). U/Pb ages of ophiolites and arc-related plutons of the Norwegian Caledonides: Implications for the development of Iapetus. Contributions to Mineralogy and Petrology, 98(1), 13–23. https://doi.org/10.1007/BF00371904
- Furnes, H., Pedersen, R. B., & Stillman, C. J. (1988). The Leka Ophiolite Complex, central Norwegian Caledonides: Field characteristics and
- geotectonic significance. Journal of the Geological Society, 145(3), 401–412. https://doi.org/10.1144/gsjgs.145.3.0401
 Gale, A., Dalton, C. A., Langmuir, C. H., Su, Y., & Schilling, J. (2012). The mean composition of ocean ridge basalts. Geochemistry, Geophysics, Geosystems, 14(3), 489–518. https://doi.org/10.1029/2012GC004334
- Gee, D. G., Fosser, H., Henriksen, N., & Higgins, A. K. (2008). From the early Paleozoic platforms of Baltica and Laurentia to the Caledonide
- orogen of Scandinavia and Greenland. *Episodes*, 31(1), 44–51. https://doi.org/10.18814/epiiugs/2008/v31i1/007
 Gerstenberger, H., & Haase, G. (1997). A highly effective emitter substance for mass spectrometric Pb isotope ratio determinations. *Chemical*
- Geology, 136(3—4), 309–312. https://doi.org/10.1016/S0009-2541(96)00033-2 Godard, M., Dautria, J.-M., & Perrin, M. (2003). Geochemical variability of the Oman ophiolite lavas: Relationship with spatial distribution and
- paleomagnetic directions. Geochemistry, Geophysics, Geosystems, 4(6), 8609. https://doi.org/10.1029/2002GC000452 Guice, G., McDonald, I., Hughes, H., Schlatter, D., Goodenough, K., MacDonald, J., & Faithfull, J. (2018). Assessing the validity of negative high
- field strength-element anomalies as a proxy for Archean subduction: Evidence from the Ben Strome Complex, NW Scotland. *Geosciences*, 8(9), 338. https://doi.org/10.3390/geosciences8090338
- Guice, G. L., Ackerson, M. R., Holder, R. M., George, F. R., Browning-Hanson, J. F., Burgess, J. L., et al. (2021). Suprasubduction zone ophiolite fragments in the central Appalachian orogen: Evidence for mantle and Moho in the Baltimore Mafic Complex (Maryland, USA). *Geosphere*, 17(2), 561–581. https://doi.org/10.1130/ges02289.1
- Guice, G. L., McDonald, I., Hughes, H. S. R., & Anhaeusser, C. R. (2019). An evaluation of element mobility in the Modderfontein ultramafic complex, Johannesburg: Origin as an Archaean ophiolite fragment or greenstone belt remnant? *Lithos*, 332–333, 99–119. https://doi.org/10.1016/j.lithos.2019.02.013
- Haller, M. B., O'Driscoll, B., Day, J. M. D., Daly, J. S., Piccoli, P. M., & Walker, R. (2021). Meter-scale chemical and isotopic heterogeneities in the oceanic mantle, Leka Ophiolite Complex, Norway. *Journal of Petrology*, 62(12), 1–29. https://doi.org/10.1093/petrology/egab061
- Hanan, B. B., & Sinha, A. K. (1989). Petrology and tectonic affinity of the Baltimore mafic complex, Maryland. In S. K. Mittwede & E. F. Stoddard (Eds.), *Ultramafic rocks of the Appalachian Piedmont, GSA special papers* (Vol. 231, pp. 1–18). Geological Society of America. https://doi.org/10.1130/SPE231-p1
- Hiess, J., Condon, D. J., McLean, N., & Noble, S. R. (2012). ²³⁸U/²³⁵U systematics in terrestrial uranium-bearing minerals. *Science*, 335(6076), 1610–1614. https://doi.org/10.1126/science.1215507
- Horstwood, M. S. A., Košler, J., Gehrels, G., Jackson, S. E., McLean, N. M., Paton, C., et al. (2016). Community-derived standards for LA-ICP-MS U-(Th-)Pb geochronology—Uncertainty propagation, age interpretation and data reporting. *Geostandards and Geoanalytical Research*, 40(3), 311–332. https://doi.org/10.1111/j.1751-908X.2016.00379.x
- Irvine, T. N., & Baragar, W. R. A. (1971). A guide to the chemical classification of the common volcanic rocks. *Canadian Journal of Earth Sciences*, 8(5), 523–548. https://doi.org/10.1139/e71-055
- Ishikawa, T., Nagaishi, K., & Umino, S. (2002). Boninitic volcanism in the Oman ophiolite: Implications for thermal condition during transition from spreading ridge to arc. *Geology*, 30(10), 899–902. https://doi.org/10.1130/0091-7613(2002)030<0899:BVITOO>2.0.CO;2
- Ishizuka, O., Tani, K., Reagan, M. K., Kanayama, K., Umino, S., Harigane, Y., et al. (2011). The timescales of subduction initiation and subsequent evolution of an oceanic island arc. *Earth and Planetary Science Letters*, 306(3—4), 229–240. https://doi.org/10.1016/j.epsl.2011. 04.006
- Jaffey, A. H., Flynn, K. F., Glendenin, L. E., Bentley, W. C., & Essling, A. M. (1971). Precision measurements of half-lives and specific activities of ²³⁵U and ²³⁸U. Physical Review C, 4(5), 1889–1906. https://doi.org/10.1103/physrevc.4.1889
- Krogh, T. E. (1973). A low contamination method for hydrothermal decomposition of zircon and extraction of U and Pb for isotopic age determination. Geochimica et Cosmochimica Acta, 37(3), 485–494. https://doi.org/10.1016/0016-7037(73)90213-5
- Kusano, Y., Umino, S., Shinjo, R., Ikei, A., Adachi, Y., Miyashita, S., & Arai, S. (2017). Contribution of slab-derived fluid and sedimentary melt in the incipient arc magmas with development of the paleo-arc in the Oman Ophiolite. *Chemical Geology*, 449, 206–225. https://doi.org/10. 1016/j.chemgeo.2016.12.012
- Laurent, R., & Hébert, R. (1989). The volcanic and intrusive rocks of the Québec Appalachian ophiolites (Canada) and their island-arc setting. Chemical Geology, 77(3—4), 287–302. https://doi.org/10.1016/0009-2541(89)90079-X
- Li, H., Arculus, R. J., Ishizuka, O., Hickey-Vargas, R., Yogodzinski, G. M., McCarthy, A., et al. (2021). Basalt derived from highly refractory mantle sources during early Izu-Bonin-Mariana arc development. *Nature Communications*, 12(1723), 1723. https://doi.org/10.1038/s41467-021.21080.0
- Ludwig, K. R. (2003a). User's manual for Isoplot 3.00. Special Publication (Vol. 4). Berkeley Geochrono.

BECKER ET AL. 18 of 20

- Ludwig, K. R. (2003b). *User's manual for Isoplot 3.00: A geochronological toolkit for Microsoft Excel* (Vol. 4). Berkeley Geochronology Center Special Publication. Berkeley, CA.
- Maaløe, S. (2005). The dunite bodies, websterite and orthopyroxenite dikes of the Leka ophiolite complex, Norway. *Mineralogy and Petrology*, 85(3–4), 163–204. https://doi.org/10.1007/s00710-005-0085-5
- McArthur, K. L., Frost, C. D., Barnes, C. G., Prestvik, T., & Nordgulen, Ø. (2014). Tectonic reconstruction and sediment provenance of a fartravelled oceanic nappe, Helgeland nappe complex, West-Central Norway. In F. Corfu, D. Gasser, & D. M. Chew (Eds.), New perspectives on the Caledonides of Scandanavia and related areas, special publication (Vol. 390(1), pp. 583–602). Geological Society. https://doi.org/10.1144/SP390.3
- Michels, A. C., McEnroe, S. A., & Fichler, C. (2018). Geophysical expression of the Leka ophiolite, Norway, modeled from integrated gravity, magnetic and petrophysical data. *Norsk Geologisk Tidsskrift*, 98, 103–125. https://doi.org/10.17850/njg98-1-07
- O'Driscoll, B., Leuthold, J., Lenaz, D., Skogby, H., Day, J. M., & Adetunji, J. (2021). Melt percolation, melt-rock reaction and oxygen fugacity in supra-subduction zone mantle and lower crust from the Leka Ophiolite Complex, Norway. *Journal of Petrology*, 62(11), 1–26. https://doi.org/10.1093/petrology/egab078
- O'Driscoll, B., Walker, R. J., Day, J. M. D., Ash, R. D., & Daly, J. S. (2015). Generations of melt extraction, melt-rock interaction and high-temperature metasomatism preserved in peridotites of the ~497 Ma Leka Ophiolite Complex, Norway. *Journal of Petrology*, 56(9), 1797–1828. https://doi.org/10.1093/petrology/egv055
- Olive, V., Hébert, R., & Loubet, M. (1997). Isotopic and trace element constraints on the genesis of a boninitic sequence in the Thetford Mines ophiolitic complex, Quebec, Canada. *Canadian Journal of Earth Sciences*, 4(9), 1258–1271. https://doi.org/10.1139/e17-100
- Paton, C., Hellstrom, J., Paul, B., Woodhead, J., & Hergt, J. (2011). Iolite: Free-ware for the visualisation and processing of mass spectrometric data. *Journal of Analytical Atomic Spectrometry*, 26(12), 2508–2518. https://doi.org/10.1039/C1JA10172B
- Paton, C., Woodhead, J. D., Hellstrom, J. C., Hergt, J. M., Greig, A., & Maas, R. (2010). Improved laser ablation U-Pb zircon geochronology through robust downhole fractionation correction. *Geochemistry, Geophysics, Geosystems*, 11(3), 36. https://doi.org/10.1029/2009GC002618
- Pearce, J. A., Lippard, S. J., & Roberts, S. (1984). Characteristics and tectonic significance of supra-subduction zone ophiolites. *Geological Society, London, Special Publications*, 16(1), 77–94. https://doi.org/10.1144/GSL.SP.1984.016.01.06
- Pearce, J. A., & Reagan, M. K. (2019). Identification, classification, and interpretation of boninites from Anthropocene to Eoarchean using Si-Mg-Ti systematics. Geosphere, 15(4), 1008–1037. https://doi.org/10.1130/ges01661.1
- Pearce, J. A., Reagan, M. K., Petronotis, K., Morgan, S., Almeev, R., Avery, A. J., et al. (2015). Izu-Bonin-Mariana fore arc: Testing subduction initiation and ophiolite models by drilling the outer Izu-Bonin-Mariana fore arc. In *Integrated ocean drilling program preliminary report*, 352. https://doi.org/10.14379/iodp.pr.352.2015
- Pedersen, R. B., Furnes, H., & Dunning, G. R. (1988). Some Norwegian ophiolite complexes reconsidered (Vol. 3, pp. 80–85). Norges Geologiske Undersøkelse Special Publication.
- Prestvik, T. (1980). The Caledonian ophiolite complex of Leka, north central Norway. In A. Panayiotou (Ed.), *Ophiolites* (pp. 555–566). Geological Survey Department.
- Prestvik, T. (1985). Origin of the volcanic Storoya group, Leka. Results from new geochemical investigations. Norsk Geologisk Tidsskrift, 65, 237-230
- Reagan, M. K., Heaton, D. E., Schmitz, M. D., Pearce, J. A., Shervais, J. W., & Koppers, A. A. P. (2019). Forearc ages reveal extensive short-lived and rapid seafloor spreading following subduction initiation. *Earth and Planetary Science Letters*, 506, 520–529. https://doi.org/10.1016/j.epsl. 2018.11.020
- Reagan, M. K., Ishizuka, O., Stern, R. J., Kelley, K. A., Ohara, Y., Blichert-Toft, J., et al. (2010). Fore-arc basalts and subduction initiation in the Izu-Bonin-Mariana system. *Geochemistry, Geophysics, Geosystems*, 11(3), 1–17. https://doi.org/10.1029/2009GC002871
- Rioux, M., Garber, J. M., Searle, M., Kelemen, P., Miyashita, S., Adachi, Y., & Bowring, S. (2021). High-precision U–Pb zircon dating of late magmatism in the Semail Ophiolite: A record of subduction initiation. *Journal of Geophysical Research: Solid Earth*, 126(5), e2020JB020760. https://doi.org/10.1029/2020JB020760
- Roberts, D. (1988). The terrane concept and the Scandinavian Caledonides: A synthesis. *Norges geologiske undersøkelse Bulletin*, 413, 93–99. Saccani, E. (2015). A new method of discriminating different types of post-Archean ophiolitic basalts and their tectonic significance using Th-Nb and Ce-Dy-Yb systematics. *Geoscience Frontiers*, 6(4), 481–501. https://doi.org/10.1016/j.gsf.2014.03.006
- Schaltegger, U., Schmitt, A. K., & Horstwood, M. S. A. (2015). U-Th-Pb geochronology by ID-TIMS, SIMS, and laser ablation ICP-MS: Recipes, interpretations, and opportunities. *Chemical Geology*, 402, 89–110. https://doi.org/10.1016/j.chemgeo.2015.02.028
- Schmitz, M. D., & Schoene, B. (2007). Derivation of isotope ratios, errors and error correlations for U-Pb geochronology using ²⁰⁵Pb-²³⁵U-(²³³U)-spiked isotope dilution thermal ionization mass spectrometric data. *Geochemistry, Geophysics, Geosystems*, 8(8), Q08006. https://doi.org/10.1029/2006GC001492
- Schoene, B., Crowley, J. L., Condon, D. J., Schmitz, M. D., & Bowring, S. A. (2006). Reassessing the uranium decay constants for geochronology using ID-TIMS U-Pb data. *Geochimica et Cosmochimica Acta*, 70(2), 426–445. https://doi.org/10.1016/j.gca.2005.09.007
- Shafaii Moghadam, H. S., Stern, R. J., Chiaradia, M., & Rahgoshay, M. (2013). Geochemistry and tectonic evolution of the Late Cretaceous Gogher–Baft ophiolite, central Iran. *Lithos*, 168–169, 33–47. https://doi.org/10.1016/j.lithos.2013.01.013
- Shervais, J. W. (1982). Ti-V plots and the petrogenesis of modern ophiolitic lavas. Earth and Planetary Science Letters, 59(1), 101–118. https://doi.org/10.1016/0012-821X(82)90120-0
- Shervais, J. W. (2001). Birth, death, and resurrection: The life cycle of suprasubduction zone ophiolites. *Geochemistry, Geophysics, Geosystems*, 2(1), 1010. https://doi.org/10.1029/2000GC000080
- Shervais, J. W., Reagan, M., Haugen, E., Almeev, R. R., Pearce, J. A., Prytulak, J., et al. (2019). Magmatic response to subduction initiation: Part 1. Fore-arc basalts of the Izu-Bonin arc from IODP expedition 352. *Geochemistry, Geophysics, Geosystems*, 20, 314–338. https://doi.org/10.1029/2018GC007731
- Shervais, J. W., Reagan, M. K., Godard, M., Prytulak, J., Ryan, J. G., Pearce, J. A., et al. (2021). Magmatic response to subduction initiation, Part II: Boninites and related rocks of the Izu-Bonin Arc from IOPD Expedition 352. *Geochemistry, Geophysics, Geosystems*, 22, 1–34. https://doi.org/10.1029/2020GC009093
- Sláma, J., Košler, J., Condon, D. J., Crowley, J. L., Gerdes, A., Hanchar, J. M., et al. (2008). Plešovice zircon—A new natural reference material for U–Pb and Hf isotopic microanalysis. *Chemical Geology*, 249(1–2), 1–35. https://doi.org/10.1016/j.chemgeo.2007.11.005
- Stern, R. J., & Bloomer, S. H. (1992). Subduction zone infancy: Examples from the Eocene Izu-Bonin-Mariana and Jurassic California arcs. Geological Society of America Bulletin, 104(12), 1621–1636. https://doi.org/10.1130/0016-7606(1992)104<1621:SZIEFT>2.3.CO;2
- Stern, R. J., Reagan, M., Ishizuka, O., Ohara, Y., & Whattam, S. (2012). To understand subduction initiation, study forearc crust: To understand forearc crust, study ophiolites. *Lithosphere*, 4(6), 469–483. https://doi.org/10.1130/L183.1

BECKER ET AL. 19 of 20

- Sturt, B. A., Andersen, T. B., & Furnes, H. (1985). The Skei Group, Leka: An unconformable clastic sequence overlying the Leka Ophiolite. In D. G. Gee & B. A. Stuart (Eds.), *The Caledonide Orogen Scandinavian and related areas* (Vol. 1, pp. 395–405). Bergen, Norway: University of Bergen, Geological Department.
- Titus, S. J., Fossen, H., Pedersen, R. B., Vigneresse, J. L., & Tikoff, B. (2002). Pull-apart formation and strike-slip partitioning in an obliquely divergent setting, Leka Ophiolite, Norway. *Tectonophysics*, 354(1—2), 101–119. https://doi.org/10.1016/S0040-1951(02)00293-7
- Tveit, R., Furnes, H., & Pedersen, R. B. (1993). Geological and geochemical development of the submarine volcanic sequence on Storøya, Leka Ophiolite Complex, North Trøndelag. *Norsk Geologisk Tidsskrift*, 73, 81–94.
- Vermeesch, P. (2018). IsoplotR: A free and open toolbox for geochronology. Geoscience Frontiers, 9(5), 1479–1493. https://doi.org/10.1016/j.gsf.2018.04.001
- Whattam, S. A., & Stern, R. J. (2011). The "subduction initiation rule": A key for linking ophiolites, intra-oceanic forearcs, and subduction initiation. Contributions to Mineralogy and Petrology, 162(5), 1031–1045. https://doi.org/10.1007/s00410-011-0638-z
- Wiedenbeck, M., Allé, P., Corfu, F., Griffin, W. L., Meier, M., Oberli, F., et al. (1995). Three natural zircon standards for U-Th-Pb, Lu-Hf, trace element and REE analyses. *Geostandards Newsletter*, 19(1), 1–23. https://doi.org/10.1111/j.1751-908X.1995.tb00147.x
- Winchester, J. A., & Floyd, P. A. (1977). Geochemical discrimination of different magma series and their differentiation products using immobile elements. *Chemical Geology*, 20(4), 325–343. https://doi.org/10.1016/0009-2541(77)90057-2
- Zhou, X., Li, Z., Gerya, T. V., Stern, R. J., Xu, Z., & Zhang, J. (2018). Subduction initiation dynamics along a transform fault control trench curvature and ophiolite ages. *Geology*, 46(7), 607–610. https://doi.org/10.1130/G40154.1

BECKER ET AL. 20 of 20